Research Square

Preprints are preliminary reports that have not undergone peer review.
They should not be considered conclusive, used to inform clinical practice,
or referenced by the media as validated information.

In Vitro and In Silico Analysis of the Anticancer Potential of Flavoparmelia caperata Lichen on Certain Cancer Cell Lines

İlayda Ünal
Yozgat Bozok University
Mehmet Ünsal Barak
mehmetu.barak@bozok.edu.tr
Yozgat Bozok University
Dilek Pandır
Yozgat Bozok University

Article

Keywords: Flavoparmelia caperata, Cancer, HPLC, MTT, Molecular docking

Posted Date: May 4th, 2026

DOI: https://doi.org/10.21203/rs.3.rs-9368688/v1

License: This work is licensed under a Creative Commons Attribution 4.0 International License.
Read Full License

Additional Declarations: No competing interests reported.

Abstract

Current methods used in cancer treatment increase the need for new and more selective anticancer agents owing to limitations such as side effects and treatment resistance. In this study, the anticancer potential of *Flavoparmelia caperata* lichen was evaluated via in vitro and in silico approaches in A549, HT-29, and HeLa cells. The extract content was analysed via HPLC, the cytotoxic effects were determined via the MTT assay, and the interactions of secondary metabolites with target proteins were investigated via molecular docking. LD_{50} values obtained from the MTT test: 62.5 µg/mL for A549 cells, 31.25 µg/mL for HT-29 cells, 62.5 µg/mL for HeLa cells, and 90 µg/mL for L929 cells. The G2/M DNA damage checkpoint by WEE1 kinase is an important target for cancer therapy, especially for cancer types deficient in p53. We examined the inhibitory potential of the lichen-derived secondary metabolites usnic acid, atranorin, and protocetraric acid against human WEE1 kinase (PDB ID: 8BJU). All three lichen acids demonstrated binding affinities ranging from −8.7 to −9.5 kcal/mol. Protocetraric acid demonstrated a maximum binding potential of −9.5 kcal/mol. ASN376 acts as an anchor point during protein−ligand interactions, forming crucial hydrogen bonds. Additionally, specific aromatic interactions with the PHE433 residue of the catalytic pocket of WEE1 kinase were observed. Lichen-derived natural compounds, especially protocetraric acid, display high specificity by forming a hydrogen-bond network that effectively targets the WEE1 kinase active site. Lichen-derived natural compounds could be effective therapeutic options against cancer types deficient in p53, especially A549, HeLa and HT-29 cancer cell lines.

INTRODUCTION

Cancer is a heterogeneous group of diseases characterized by the uncontrolled proliferation of abnormal cells that can occur in any tissue or organ of the body. These cells can invade surrounding tissues over time and metastasize to distant organs, seriously worsening the prognosis of the disease. The metastasis process is considered one of the fundamental biological mechanisms determining cancer mortality (Mathur et al. 2020, Hardell and Nilsson 2025).

Cancer remains a major health concern for people around the World, emphasizing the need for the discovery of new therapeutic drugs that can selectively target the underlying causes of cancer. Among the new strategies adopted in the treatment of cancer, the strategy of targeting cell cycle checkpoints has shown promising results (Kaur et al. 2023). The G2/M DNA damage checkpoint is a critical regulatory checkpoint that maintains genomic stability and prevents damaged cells from entering mitosis. WEE1 kinase is a major player in this checkpoint and phosphorylates and inactivates the Cdc2/cyclin B complex. This forces the cell to arrest in the G2 phase. In many cancers, especially those with a mutated p53 gene, the G1 checkpoint is defective. These cells are heavily dependent on the G2/M checkpoint and thus the WEE1 pathway. This has made the WEE1 pathway an interesting target for intervention because its inhibition forces the cell to enter premature mitosis and die (Bukhari et al. 2022).

Despite the clinical progress made with several synthetic WEE1 inhibitors, such as AZD1775 (adavosertib), there is a constant need to identify new lead compounds from natural products that are known for their high specificity, low systemic toxicity, and unique chemical structure (Alli et al. 2023). Lichens are composite organisms formed between fungi and either algal or cyanobacterial photobionts (Patil and Gore, 2025). Lichens are known for their high diversity of unique secondary metabolites with a range of biological activities, including antioxidant, antimicrobial, and anticancer properties. The lichen secondary metabolites usnic acid, atranorin, and protocetraric acid are reported to possess considerable cytotoxic activity against various human cancer cell types (Suresh and Nadumane, 2026). The molecular mechanisms underlying these interactions with important cell cycle regulators, such as human WEE1 kinase are not well understood (Zhang et al. 2025). In our present study, we used an in silico molecular docking method to investigate the inhibitory activity of these three important lichen secondary metabolites against human WEE1 kinase. Using the crystal structure of the human WEE1 kinase (PDB ID: 8BJU), we attempted to elucidate the binding affinity and interaction network of usnic acid, atranorin, and protocetraric acid with ATP binding site of the human WEE1 kinase. In addition, we used a comparative docking model with a reference ligand QT9 that had been cocrystallized with the human WEE1 kinase to validate our docking model and assess its competitiveness.

Lung cancer ranks among the malignancies with the highest incidence and mortality rates globally. According to data from the Global Cancer Observatory (GLOBOCAN), it was the most commonly diagnosed cancer worldwide in 2022, with approximately 2.5 million new cases. (Sung et al. 2021). Furthermore, as of 2024, lung cancer continues to be the leading cause of cancer-related death among both women and men in the United States. (Siegel et al. 2024). This high disease burden necessitates the development of effective preventive measures and new treatment strategies (Ferlay et al. 2021).

Colorectal cancer (CRC) refers to malignant neoplasms that develop in the colon and rectum and is particularly prevalent in developed countries. It is reported as the third most common cancer type in both sexes in the United States. Globally, approximately 1.93 million new cases were reported in 2020, and approximately 940,000 deaths occurred due to this disease. These data reveal that colorectal cancer accounts for approximately 10% of cancer cases worldwide (Pacal et al. 2020; Sung et al. 2021).

Cervical cancer is a significant malignancy, particularly in terms of women's health, and is notable for its high mortality rates in developing countries. According to World Health Organization data, cervical cancer causes the death of one woman every two minutes and ranks second among the most common types of cancer in women. High-risk human papillomavirus (HPV) types, particularly HPV-16 and HPV-18, play a fundamental role in the etiology of this disease. These viral types trigger malignant transformation in cervical cells by inactivating the tumor suppressor proteins p53 and Rb via the E6 and E7 oncoproteins (Turanlı, 2021; Adigun et al. 2023; Alshehri et al. 2023).

Methods used in cancer treatment are generally classified into conventional and modern approaches. Although traditional methods such as surgery, chemotherapy, and radiotherapy are still widely used, the toxic effects of chemotherapy and radiotherapy on healthy tissues pose significant limitations. The fact

that chemotherapeutic agents also target rapidly dividing healthy cells has lead to the emergence of severe side effects (Debela et al. 2021). This situation has increased interest in more specific and less toxic modern treatment strategies such as targeted therapies, immunotherapies, and antiangiogenic agents (Tripathi et al. 2021). In recent years, the side effects caused by synthetic anticancer drugs and the development of drug resistance have accelerated research into naturally derived compounds. In this context, lichens, which are rich in secondary metabolites, are among the organisms that are noteworthy in terms of the discovery of potential anticancer agents (Manojlović et al. 2021).

Lichens are organisms that form a symbiotic association between fungi and green algae (Chlorophyta) and/or cyanobacteria (Cyanobacteria). They are widely distributed throughout the world and can live on various substrates. Lichens, considered one of the most successful examples of symbiotic life in nature, develop within a framework of physiological division of labor, with photosynthetic partners meeting the nutritional needs of lichens, while the fungal component provides these organisms with a protected living space (Spribille et al. 2022). Owing to this mutually beneficial relationship, lichens have gained the ability to survive for long periods even in habitats dominated by extreme environmental conditions (Güvenç et al. 2020). However, the fact that the algal partner within the symbiotic structure has greater growth capacity in its free-living form suggests that the lichen association could also be considered controlled parasitism (Morillas et al. 2022).

Lichens, which are capable of both asexual and sexual reproduction, are classified taxonomically within the fungal kingdom (Fungi) because their sexual reproductive structures are formed by the fungal component. The majority of fungi that form lichens belong to the Ascomycota division, whereas a smaller portion belong to the Basidiomycota division (Tripp et al. 2018; Steinová et al. 2019). Lichens, which have wide ecological tolerances ranging from tropical rainforests to arid deserts and polar regions, contribute significantly to ecosystem processes such as nutrient cycling, soil formation, and microhabitat diversity by spreading throughout all terrestrial ecosystems owing to their cosmopolitan distribution (Spribille et al. 2022). One of the most important characteristics that distinguish lichens from other organisms is their ability to produce rich metabolites that serve a protective function against environmental stress factors. Lichen metabolites are divided into two groups: primary and secondary. Secondary metabolites generally constitute 0.1–10% of dry weight, although in some species this proportion can reach 30% (Lawrey, 1986; Furmanek et al. 2019). These compounds accumulate within the lichen thallus, mostly on the surface of fungal hyphae, in the form of crystalline or amorphous structures (Stanojkovic, 2019). To date, more than 1,000 secondary metabolites unique to lichens have been identified, and these compounds have been widely applied in the perfume, cosmetic, paint, food, and especially pharmaceutical industries (Felczykowska et al. 2017). These secondary metabolites, which possess a wide range of pharmacological activities, such as antimicrobial, antioxidant, antiviral, anticancer, antigenotoxic, anti-inflammatory, analgesic, and antipyretic properties, make lichens important biological resources in natural product-based drug discovery and development studies (Ranković, 2019; Solárová et al. 2020).

In silico approaches, particularly molecular docking analyses, are emerging as important tools in the drug discovery process for understanding the biological activities of lichen secondary metabolites at the molecular level. Molecular docking studies provide significant advantages in terms of time and cost by guiding experimental studies by predicting the binding modes and binding affinities of small molecules with target proteins (Gaikwad et al. 2023; Das et al. 2025).

Flavoparmelia caperata (L.) Hale is a lichen species with a foliose structure, that is yellow–green in color and expands to a diameter of 5–20 cm, with lobes that are semi-irregular and smooth. Usnic acid and atranorin are found in the upper cortex, whereas protocetraric and caperic acid are found in the medulla. Soredia are laminal and granular in structure, and isidia are absent. This species is found in open areas with broad-leaved trees, shrubs, and occasionally rocks at elevations of up to 2000 m (Nash III et al. 2002).

Evaluating the effects of secondary metabolites derived from lichens on different types of cancer through molecular binding studies offers an important approach for identifying promising lead compounds for lung, colon, and cervical cancers. In this study, the amounts of usnic acid, atranorin, and protocetraric acid compounds present in the extracts obtained from *F. caperata* lichens were determined via high-performance liquid chromatography (HPLC). Additionally, the anticancer potential of these metabolites has been evaluated at the molecular level in A549 lung cancer, HT-29 colon cancer, HeLa cervical cancer, and healthy L929 mouse fibroblast lines. The molecular docking analyses performed aimed to elucidate the interaction mechanisms of the lichen metabolites in question with cancer-related target proteins and to reveal their potential cell line-specific biological activities.

MATERIALS AND METHODS

Collection of lichens

A sample of the lichen species *F. caperata* was collected on April 28, 2024, from the Yenice Forests in Karabük Province during fieldwork at an elevation of 350 m, at coordinates 41°07'16.4" N 32°16'57.6" E, from *Fagus orientalis* Lipsky (Fig. 1).

The lichen species were identified by Dr. Mehmet Ünsal Barak according to the studies of Brodo et al. (2001) and Nash III et al. (2002). The voucher specimen (Herbarium No. MUB 0.371) has been deposited in the Bozok Herbarium. The necessary legal permits for the collection of lichen specimens were obtained. All procedures related to lichen samples were conducted in accordance with national, international, and institutional guidelines and legislation.

Extraction of lichen

Ten grams of the prepared lichen samples were weighed and ground in a mortar under sterile conditions until they became powder. The powdered lichen samples obtained were extracted via an 70% methanol

solution on the basis of the protocol developed by Kocakaya et al. (2021). Following the extraction process, the obtained extracts were filtered and concentrated under low pressure using a rotary evaporator. The resulting dry lichen extracts were stored at -20°C for use in experimental studies (Kocakaya et al. 2021).

Prior to experimental application, dry extracts were dissolved in 70% ethanol; subsequent dilution to appropriate concentrations was performed via Dulbecco's Modified Eagle Medium (DMEM) and Roswell Park Memorial Institute (RPMI) media. Prior to applying the extracts to the cell culture medium, the samples were purified by filtration through a sterile membrane filter with a pore size of 0.22 microns to prevent any dirty appearance and possible unwanted interactions that could occur due to particle accumulation.

Determination of lichen acids content via HPLC

The HPLC analyser used for analysis was an Agilent Technologies 1260 Infinity series model. The dry powder lichen samples to be analysed were prepared by dissolving the mobile phase prepared for HPLC. The unsolved portions of the samples were prepared for injection via 0.45 µm membrane filters. The detector used for HPLC analysis was a DAD detector, and the wavelength used was set to 240 nm. The mobile phase consisted of a methanol-water-acetic acid (85:15:5, v/v/v) mixture. The analysis was performed using a C18 column (USEM Arge brand – 5 µm, 150 mm × 4.6 mm). During the analysis, the mobile phase flow rate was set at 1 mL/min. The standards used were prepared by dissolving them in a mobile phase solution. The specified concentrations were 20 ppm, 10 ppm, and 2 ppm.

Determination of the cytotoxic effects of lichen extract via the MTT method

The cells were seeded into 96-well flat-bottom sterile cell culture plates, with $1x10^4$ cells added to each well to allow the cells to proliferate. After plating, the plates were left for a 24-hour incubation period for cell adaptation and proliferation. At the end of the incubation period, different doses of *F. caperata* lichen were applied to the cells. The doses of the lichens were diluted with the culture medium and added. The control group was created by adding only the culture medium, and the same volume of culture medium was added to ensure the control conditions of the experiment.

A 48-hour incubation period was used to evaluate the effects of the lichens on the cells. At the end of this incubation period, 25 µl of MTT solution was added to all the wells, including the control group, and incubated for 2.5 hours. Then, 150 µl of solubilization buffer (Roche) was added to each well, and the mixture was incubated for 2 hours to dissolve the formazan crystals. At the end of the 2-hour incubation period, the plates were gently shaken, and spectrophotometric measurements were taken at a wavelength of 570 nm. LD_{50} doses were calculated by analysing the decrease rates in cell viability on the basis of the obtained absorbance data.

Protein and ligand preparation

To identify the potential biological targets of the lichen secondary metabolites under investigation, namely usnic acid, atranorin, and protocetraric acid, an in silico approach was used to predict the targets of these compounds via the SwissTargetPrediction server tool (Daina et al. 2019). The predictions revealed a remarkable common characteristic of the three compounds, which was the ability of the compounds to interact with the kinase family of proteins, with the percentages of atranorin, protocetraric acid, and usnic acid binding to the kinase family of proteins being 20.0%, 46.7%, and 13.3%, respectively (Fig. 2).

Considering the central position of kinases in the proliferation of cancer cells, as well as signal transduction pathways, kinases have been identified as a highly druggable family of enzymes. On the basis of the common bioactivity profile of the three lichen acids, WEE1 kinase (PDB code: 8BJU), a central player in the G2/M checkpoint of the cell cycle, as well as a highly promising target in oncology, has been identified as the representative kinase target for the molecular docking simulation, given the common bioactivity profile of the three lichen acids, which points to kinase inhibition as a potential mechanism of action of these compounds.

The crystal structure of the human WEE1 kinase in complex with its inhibitor was obtained from the Protein Data Bank (PDB) RCSB database, and the PDB code used in the study is 8BJU. Before the docking process, the protein was prepared by deleting the crystal water molecules, ions, and ligands that were already present in the crystal structure. The missing heavy atoms and polar hydrogen were added to the protein, and the receptor was assigned Kollman charges. The three-dimensional structures of the lichen secondary metabolites, namely, usnic acid, atranorin, and protocetraric acid, were obtained, and the geometry was optimized via the UCSF Chimera software for the refinement of the ligands (Pettersen et al. 2004). All the compounds were converted to the PDBQT format for the docking process.

Molecular docking protocol

The docking simulations were performed by employing the AutoDock Vina 1.2.0 protocol, where the binding site for the ligands was defined by specifying the coordinates of the center of the grid box to coincide with the coordinates of the cocrystallized ligand, namely, QT9, to ensure that the whole binding site, including the crucial residues ASN376 and PHE433, was included in the grid box (Eberhardt et al. 2021). Molecular docking calculations were performed using a grid size of 40 × 40 × 40 $Å^3$. This grid is centered at x: -14.097, y: -11.124, and z: 19.319 with a grid spacing of 0.375 Å. In addition, an exhaustiveness of 64 is used. The best binding affinity for the ligand, represented by the most negative score, was used for the interaction studies.

Validation of the docking procedure

To validate the accuracy of the docking protocol, a redocking study was carried out by extracting the reference ligand QT9 from the 8BJU protein crystal structure and redocking it into its defined active site. The high binding affinity for QT9 and its interaction with key residues confirmed the accuracy of the docking protocol.

Visualization and interaction analysis

The protein–ligand complexes were visualized and analysed by employing BIOVIA Discovery Studio Visualizer 4.0 (BIOVIA - Dassault Systèmes, 2026). Two-dimensional interaction diagrams were employed to identify and classify noncovalent interactions, conventional hydrogen bonds, π–π stacking, π–alkyl interactions, and van der Waals forces. This analysis of interaction distances and active site residues was used to evaluate the inhibitory potential of lichen-derived metabolites against the target protein.

Statistical analysis

All the statistical analyses were performed via one-way analysis of variance (ANOVA) and Tukey's test via the SPSS 11.5 software package. According to the analysis results, a p-value < 0.05 was considered statistically significant.

RESULTS

HPLC analysis

As a result of the HPLC analyses performed, three major secondary metabolites were identified in the *F. caperata* lichen sample: usnic acid, protocetraric acid, and atranorin (Fig. 3).

Usnic acid stood out as the compound present in the highest proportion in the sample, with a retention time of 19,181 minutes and a concentration of 800 ppm. Considering the peak area of 2.82034×10^{4} mAU·s and the calibration factor of 2.83654×10^{-2}, usnic acid plays a dominant and central role in the biochemical composition of *F. caperata*. Protocetraric acid was identified with a retention time of 7.496 minutes and detected at a concentration of 200 ppm. The peak area for the compound was determined to be 5361.30041 mAU·s, and the calibration factor was determined to be 3.73044×10^{-2}. These data indicate that protocetraric acid is present at a significant level in the secondary metabolite profile of *F. caperata*. Atranorin was detected with a retention time of 21.840 minutes and measured at a level of 350 ppm. Considering the peak area of 2.46380×10^{4} mAU·s and the calibration factor of 1.42057×10^{-2}, atranorin was the second compound with the highest concentration after usnic acid. These results demonstrate that atranorin also plays an important role in the metabolite composition of lichens (Table 1).

Table 1

Qualitative and quantitative HPLC-UV analysis of the secondary metabolite profile in *Flavoparmelia caperata* lichen extract. The table details the identified compounds, including usnic acid (UA), atranorin (AT), and protocetraric acid (PCA), with their respective retention times (min), peak areas (mAU·s), concentrations (ppm), and specific calibration factors used for the quantification of each metabolite within the extract.

Compound Name	Retention Time (min.)	Concentration (ppm)	Peak Area (mAU·s)	Calibration Factor
Usnic acid	19,181	800	$2{,}82034 \times 10^{4}$	$2{,}83654 \times 10^{-2}$
Protocetraric acid	7,496	200	5361,30041	$3{,}73044 \times 10^{-2}$
Atranorin	21,840	350	$2{,}46380 \times 10^{4}$	$1{,}42057 \times 10^{-2}$

MTT analysis

On the basis of the results of the MTT test conducted in accordance with the application doses specified in Table 2, the cytotoxic effects of *F. caperata* lichen extract on the A549, HT-29, HeLa, and L929 cell lines were evaluated. On the basis of the data obtained, the LD_{50} (the dose causing the death of 50% of the tested cell population) and LD_{100} (the dose causing the death of the entire tested population) values were calculated for each cell line and are presented in Table 2.

Table 2

Comparative evaluation of the in vitro cytotoxic potential of *Flavoparmelia caperata* extract on diverse human cancer and healthy cell lines. The data present the LD_{50} and LD_{100} values (measured in µg/mL) obtained via the MTT assay after 24 hours of exposure to the A549 (lung carcinoma), HT-29 (colorectal adenocarcinoma), HeLa (cervical cancer), and L929 (healthy mouse fibroblast) cell lines, highlighting the selectivity of the extract.

Cell Line	A549	HT-29	HeLa	L929
LD_{50}	62,5 µM	31,25 µM	62,5 µM	90 µM
LD_{100}	125 µM	62,5 µM	125 µM	180 µM

The LD_{50} and LD_{100} values of *F. caperata* lichen extract for the A549, HT-29, and HeLa cancer cell lines were found to be effective at lower doses than the LD_{50} and LD_{100} values for the healthy fibroblast L929 cell line (Figs. 4–7).

Molecular docking analysis

To identify the binding modes and inhibitory potential of specific lichen secondary metabolites, viz., protocetraric acid, atranorin, and usnic acid, against human WEE1 kinase, a molecular docking study was performed. By employing the crystal structure of WEE1 kinase with its inhibitor (PDB ID: 8BJU), docking

simulations were performed to identify the thermodynamic stability and molecular interaction of these natural compounds with the ATP-binding domain of the target protein. The calculated binding affinities of the docked compounds ranged from –8.7 to –9.5 kcal/mol, which confirmed that these natural compounds bind spontaneously with the target protein.

Protocetraric acid (PA): PA demonstrated the highest binding affinity of –9.5 kcal/mol, which is comparable with that of the reference inhibitor. The negative value of the calculated binding energy confirmed that PA has superior geometric and electrostatic complementarity with the catalytic domain of WEE1 kinase. Moreover, hydrogen bonding with ASN376 (3.83 Å), CYS379 (3.78 Å), and SER383 (3.99 Å) was found to be robust. Additionally, C-H bonds with GLY382 (3.63 Å) and hydrophobic interactions, including Pi-Sigma interactions with ILE305 (5.21 Å) and Pi-alkyl interactions with ALA326 (5.81 Å) and VAL313 (4.78 Å), were found to be stable (Figs. 8–10).

Atranorin (AT): The compound had a binding affinity of –8.8 kcal/mol. It was stabilized through a hydrogen bond network with ASN376 (4.01 Å and 4.78 Å). There was also a strong interaction with LYS328 (4.60 Å). In addition, a unique interaction with GLU346 (5.23 Å) was noted. The aromatic ring of the compound was also stabilized through Pi-Sigma interactions with ILE305 (5.50 Å). Pi-alkyl interactions were also observed with VAL313 (4.66 Å) and ALA326 (5.66 Å). These interactions indicate the extensive occupation of the hydrophobic pocket (Figs. 11–13).

Usnic acid (UA): The compound had a binding affinity of –8.7 kcal/mol. It was stabilized through four conventional hydrogen bonds with ASN376 (4.06 Å and 5.29 Å) and ASP463 (3.49 Å and 4.32 Å). The unique features of the compound included a secondary hydrogen bond with both ASN376 and ASP463. In addition, a unique Pi–Pi T-shaped interaction was observed with PHE433 (6.69 Å). This interaction is recognized as strong kinase–inhibitor complexes. This finding is an indication of the ability of the compound to effectively compete with endogenous ATP for the kinase's active site. The interaction was further complemented by a C–H bond with GLY306 (4.27 Å) (Figs. 14–16).

Validation of the docking protocol and comparative analysis

To validate the reliability of the results obtained from the molecular docking simulations, a redocking experiment was performed by redocking the cocrystallized reference inhibitor QT9 in the active site of the WEE1 kinase enzyme (PDB code: 8BJU). The binding orientation of the reference inhibitor, QT9, also showed significant interactions with the enzyme, including conventional hydrogen bonding with ASN376 (4.25 A) and CYS379 (3.44 A) and potent aromatic interactions with PHE433 (5.74 A). This finding indicates that the docking protocol used in the study is quite accurate, as the results obtained by the docking protocol correlate quite well with the actual crystal structures of the enzyme–inhibitor complex.

The results obtained in the present study indicate that lichen-derived secondary metabolites bind to the same binding pocket as the potent inhibitor QT9 in the WEE1 kinase enzyme. Compared with the potent

inhibitor QT9, the lichen acid formed more conventional hydrogen bonds. For example, both protocetraric acid and atranorin formed more conventional hydrogen bonds with enzyme residues, such as ASN376, LYS328, and SER383, than did the potent inhibitor QT9. The repeated formation of hydrogen bonds with the residue ASN376 in the case of lichen acids and the potent inhibitor QT9 indicates that the residue plays an important role in the inhibition of the WEE1 kinase enzyme. Furthermore, the formation of Pi interactions with the residue PHE433 in the case of both usnic acid and the potent inhibitor QT9 indicates that the two molecules share similar structural features in the context of inhibition.

ADMET profiling and drug-likeness analysis

To determine the pharmacokinetic properties of the investigated lichenic acids, an extensive evaluation was performed by using the ADMETlab 3.0 tool. The results revealed that usnic acid, atranorin, and protocetraric acid adhere to Lipinski's rule of five, as there are no violations of the given rule. Notably, the high natural product (NP) scores for the investigated compounds (1.804, 0.904, and 1.830 for usnic acid, atranorin, and protocetraric acid, respectively) emphasize the potential of the investigated lichenic acids as biocompatible, natural origin drug candidates. With respect to the absorption-related properties, the investigated compounds exhibit high human intestinal absorption (HIA), as the calculated probabilities for the investigated compounds are relatively low. Additionally, the relatively low probability of crossing the blood–brain barrier (BBB) minimizes the potential for central nervous system-related side effects, thus emphasizing the therapeutic potential of the investigated lichen acids as effective WEE1 kinase inhibitors (Table 3) (Daina et al. 2017).

Table 3
Comprehensive ADMET (absorption, distribution, metabolism, excretion, and toxicity) and drug-likeness profiling of the major lichen metabolites. Systematic evaluation of usnic acid, atranorin, and protocetraric acid, including their physicochemical properties, Lipinski's rule of five compliance, synthetic accessibility, and predicted oral bioavailability for pharmaceutical development, was performed via the ADMETlab 3.0 platform.

Property	Usnic Acid (UA)	Atranorin (AT)	Protocetraric Acid (PCA)	Optimal Range / Comment
Molecular Weight	344.09	374.1	374.06	100 ~ 600
LogP (Hydrophobicity)	2.837	3.534	2.248	< 5
H-Bond Acceptors	7.0	8.0	9.0	0–12
H-Bond Donors	2.0	3.0	4.0	0–7
Lipinski Rule	0	0	0	≤ 1 violation
NP Score (Naturalness)	1.804	0.904	1.830	-5 to 5
HIA (Intestinal Abs.)	0.003	0.136	0.153	< 0.3 (High Abs.)
BBB Penetration	0.021	0.018	0.001	< 0.1 (Low Pen.)

*Data were generated via the ADMETlab 3.0 platform; probability values for HIA and BBB denote the likelihood of being category positive.

The physicochemical characteristics and potential for oral bioavailability of the compounds were represented graphically via bioavailability radar plots. As shown in Fig. 17, all three lichen acids, namely, UA, AT, and PCA, are within the desired range. BOILED-Egg was used to assess the potential gastrointestinal absorption and brain penetration of the compounds. The positioning of the compounds in the high absorpt regions on the BOILED-Egg diagram further confirms the favorable pharmacokinetic profiles of the compounds, as depicted in Fig. 18 (Daina and Zoete, 2016).

DISCUSSION

As a result of this study, it was determined that the *F. caperata* lichen species possesses a rich secondary metabolite profile. Usnic acid, detected at particularly high concentrations, has strong therapeutic potential from a biological perspective. Furthermore, the presence of other compounds, such as protocetraric acid and atranorin, indicates that *F. caperata* may be a noteworthy natural resource for pharmaceutical research.

The results of MTT assay clearly demonstrated that the cytotoxic effects of *F. caperata* lichen extract on cancer and normal cell lines were döşe dependent. Accordingly, the LD_{50} value for the A549 (lung cancer) cell line was 62.5 µg/mL, and the LD_{100} value was 125 µg/mL; for the HT-29 (colon cancer) cell line, the LD_{50} value was 31.25 µg/mL, and the LD_{100} value was 62.5 µg/mL; for the HeLa (cervical cancer) cell line, the LD_{50} value was 62.5 µg/mL, and the LD_{100} value was 125 µg/mL; and for the L929 (normal fibroblast) cell line, the LD_{50} value was 90 µg/mL and the LD_{100} value was 180 µg/mL. These data demonstrate that *F. caperata* exhibits more selective cytotoxicity against cancer cells than against normal cells. Additionally, because it has the lowest LD_{50} and LD_{100} values, HT-29 (colon cancer) was determined to be the cell line most effectively affected by *F. caperata*.

The molecular docking simulations carried out in this study provide a comprehensive account of the manner in which lichen secondary metabolites interact with the human WEE1 kinase. This protein is an important G2/M cell cycle checkpoint controller. The binding affinities of the natural compounds vary between −8.7 and −9.5 kcal/mol. This finding demonstrates a strong thermodynamic preference for natural compounds to bind to the catalytic site of the WEE1 protein.

The major finding of this analysis was the consistent involvement of ASN376 in the maintenance of all protein−ligand complexes. The ASN376 residue in the 8BJU crystal structure is located in a crucial region of the ATP-binding site. The capacity of this residue to maintain hydrogen bonds with protocetraric acid (3.83 Å), atranorin (4.01 Å), and usnic acid (4.06 Å) points toward a common mode of competitive inhibition. This ‘hot-spot’ residue could be vital in the maintenance of the inhibitors in a manner that prevents the phosphorylation of downstream targets.

The superior affinity of protocetraric acid (–9.5 kcal/mol) may be explained by the unique set of interactions. Unlike the reference ligand QT9, which uses hydrophobic packing and aromatic interactions with PHE433, protocetraric acid forms a tight cluster of hydrogen bonds with CYS379 (3.78 Å) and SER383 (3.99 Å). These results show that, unlike synthetic inhibitors, which are usually designed for hydrophobic interactions, natural lichen compounds may offer similar specificity through polar interactions.

The interaction with PHE433 in the case of usnic acid and the reference ligand QT9 via Pi–Pi T-shaped stacking at 6.69 Å also highlights the importance of aromatic amino acids in the hinge region in maintaining the structural integrity of the protein–ligand complex. The capacity of lichen acids to mimic the footprint of a potent synthetic inhibitor such as QT9 is strong evidence for the potential of these compounds in cancer treatment. In cancer treatment, the inhibition of WEE1 is useful in p53-deficient cancer cells because it forces cancer cells to undergo premature mitosis with unrepaired DNA damage, resulting in cell death.

The pronounced cytotoxic effects of the *F. caperata* lichen species, particularly on certain human cancer cell lines, provide strong evidence that these species may be potential therapeutic agent candidates. The fact that *F. caperata* can suppress the proliferation of cancer cells even at low doses suggests that the secondary metabolites found in this species contain compounds worthy of pharmacological evaluation. On the basis of these findings, it is necessary to investigate other lichen species found in Turkey for their potential anticancer properties in a similar manner. Such comprehensive studies could open new horizons in the fields of lichen biochemistry and pharmacology and could make significant contributions to the development of new-generation therapeutic agents that could be used in cancer treatment in the long term. Therefore, the primary objective of this research is not only to demonstrate the anticancer activity of *F. caperata* but also to contribute to the understanding of the biological potential of lichen species, thereby pioneering the investigation of alternative natural resources for cancer treatment.

Declarations

Competing interests

The authors declare no competing interests.

Funding

This study was supported by the Yozgat Bozok University Scientific Research Projects Coordination Unit (FYL-2025-1497).

Author Contribution

IU: Writing – review & editing, Writing – original draft, Validation, Funding acquisition, Data curation, Conceptualization, Methodology, Investigation.MUB: Writing – review & editing, Writing – original draft, Visualization, Software, Methodology, Investigation, Validation, Data curation, Conceptualization.DP: Writing – review & editing, Writing – original draft, Methodology, Investigation, Conceptualization, Validation, Funding acquisition.

Acknowledgement

We thank the Yozgat Bozok University Scientific Research Projects Coordination Unit for their financial support.

Data Availability

All data supporting the findings of this study are available within the paper.

References

1. Adıgün, M. O., Esan, D. T., Adeyanju, B. T. & Oyinloye, B. E. The role of nurses in the prevention of cervical cancer: Cervical screening, an unkept promise by the majority of women in Nigeria. *J. Integr. Nurs.* **5** (4), 311–316. https://doi.org/10.4103/jin.jin_65_23 (2023).
2. Alli, V. J., Yadav, P., Suresh, V. & Jadav, S. S. Synthetic and medicinal chemistry approaches toward WEE1 kinase inhibitors and its degraders. *Acs Omega*. **8** (23), 20196–20233. https://doi.org/10.1021/acsomega.3c01558 (2023).
3. Alshehri, M. A., Fahim, W. A. & Alsaigh, R. R. The association between parents' knowledge about human papillomavirus and their intention to vaccinate their daughters: A cross-sectional study. *Cureus* **15** (11), e48600. https://doi.org/10.7759/cureus.48600 (2023).
4. BIOVIA-Dassault Systèmes. Dassault Systèmes. (2026). https://www.3dsbiovia.com/
5. Brodo, I. M., Sharnoff, S. D. & Sharnoff, S. *Lichens of north America* (Yale University Press, 2001).
6. Bukhari, A. B., Chan, G. K. & Gamper, A. M. Targeting the DNA damage response for cancer therapy by inhibiting the kinase Wee1. *Front. Oncol.* **12**, 828684. https://doi.org/10.3389/fonc.2022.828684 (2022).
7. Daina, A. & Zoete, V. A boiled-egg to predict gastrointestinal absorption and brain penetration of small molecules. *ChemMedChem* **11** (11), 1117–1121. https://doi.org/10.1002/cmdc.201600182 (2016).
8. Daina, A., Michielin, O. & Zoete, V. SwissADME: a free web tool to evaluate pharmacokinetics, drug-likeness and medicinal chemistry friendliness of small molecules. *Sci. Rep.* **7** (1), 42717. https://doi.org/10.1038/srep42717 (2017).

9. Daina, A., Michielin, O. & Zoete, V. SwissTargetPrediction: updated data and new features for efficient prediction of protein targets of small molecules. *Nucleic Acids Res.* 47 (W1), W357-W364. (2019). https://doi.org/10.1093/nar/gkz382
10. Das, S. et al. In-silico inquest reveal the efficacy of Usnea longissima ach. (A tropical Lichen) against ovarian cancer. *Silico Pharmacol.* **13** (2), 116. https://doi.org/10.1007/s40203-025-00408-3 (2025).
11. Debela, D. T. et al. New approaches and procedures for cancer treatment: Current perspectives. *SAGE Open. Med.* **9**, 20503121211034366. https://doi.org/10.1177/20503121211034366 (2021).
12. Eberhardt, J., Santos-Martins, D., Tillack, A. F., Forli, S. & AutoDock Vina 1.2. 0: new docking methods, expanded force field, and python bindings. *J. Chem. Inf. Model.* **61** (8), 3891–3898. https://doi.org/10.1021/acs.jcim.1c00203 (2021).
13. Felczykowska, A., Pastuszak-Skrzypczak, A., Pawlik, A., Bogucka, K. & Herman-Antosiewicz, A. Guzow-Krzemińska, B. Antibacterial and anticancer activities of acetone extracts from in vitro cultured lichen-forming fungi. *BMC Complement. Altern. Med.* **17**, 1–12. https://doi.org/10.1186/s12906-017-1819-8 (2017).
14. Ferlay, J. et al. Cancer statistics for the year 2020: An overview. *Int. J. Cancer*. **149** (4), 778–789. https://doi.org/10.1002/ijc.33588 (2021).
15. Furmanek, Ł., Czarnota, P. & Seaward, M. R. D. Antifungal activity of lichen compounds against dermatophytes: A review. *J. Appl. Microbiol.* **127** (2), 308–325. https://doi.org/10.1111/jam.14209 (2019).
16. Gaikwad, S. B. et al. In vitro and in silico studies of lichen compounds atranorin and salazinic acid as potential antioxidant, antibacterial and anticancer agents. *Chem. Biodivers.* **20** (12), e202301229. https://doi.org/10.1002/cbdv.202301229 (2023).
17. Güvenç, Ş., John, V. & Türk, A. Phytogeographical analysis of the lichens and lichenicolous fungi of Turkey. *Borziana* 1, 87–108. (2020). https://doi.org/10.7320/Borz.001.087
18. Hardell, L., Nilsson, M. A. & Critical Analysis of the World Health Organization (WHO) Systematic Review. 2024 on Radiofrequency Radiation Exposure and Cancer Risks. *J. Cancer Sci. Clin. Ther.* **9**, 9–26. https://doi.org/10.26502/jcsct.5079261 (2025).
19. Kaur, R., Bhardwaj, A. & Gupta, S. Cancer treatment therapies: traditional to modern approaches to combat cancers. *Mol. Biol. Rep.* **50** (11), 9663–9676. https://doi.org/10.1007/s11033-023-08809-3 (2023).
20. Kocakaya, Z., Kocakaya, M. & Şeker Karatoprak, G. Comparative analyses of antioxidant, cytotoxic, and anti-inflammatory activities of different Cladonia species and determination of fumarprotocetraric acid amounts. *KSU J. Agric. Nat.* **24** (6), 1196–1207. https://doi.org/10.18016/ksutarimdoga.vi.868927 (2021).
21. Lawrey, J. D. Biological role of lichen substances. *Bryologist* **89** (2), 111–122. https://doi.org/10.2307/3242751 (1986).
22. Manojlović, N. T., Rančić, A. B., Décor, R., Vasiljević, P. & Tomović, J. Determination of chemical composition and antimicrobial, antioxidant and cytotoxic activities of lichens Parmelia conspersa

and Parmelia perlata. *J. Food Meas. Charact.* **15**, 686–696. https://doi.org/10.1007/s11694-020-00672-1 (2021).

23. Mathur, P. et al. Cancer statistics, 2020: report from national cancer registry programme, India. *JCO Glob Oncol.* **6**, 1063–1075. https://doi.org/10.1200/GO.20.00122 (2020).
24. Morillas, L., Roales, J., Cruz, C. & Munzi, S. Lichen as multipartner symbiotic relationships. *Encyclopedia* **2** (3), 1421–1431. https://doi.org/10.3390/encyclopedia2030096 (2022).
25. Nash, I. I. I., Ryan, T. H., Gries, B. D., Bungartz, F. & C. & *Lichen flora of the Greater Sonoran Desert region* (Lichens Unlimited, Arizona State University, 2002).
26. Pacal, I., Karaboga, D., Basturk, A., Akay, B. & Nalbantoglu, U. A comprehensive review of deep learning in colon cancer. *Comput. Biol. Med.* **126**, 104003. https://doi.org/10.1016/j.compbiomed.2020.104003 (2020).
27. Patil, P. S. & Gore, N. S. Botanical Symbiosis Unveiled: A Review of Mycorrhizas, Lichen, and Plant Consorts: PS Patil. *Bot. Rev.* **91** (2), 103–126. https://doi.org/10.1007/s12229-025-09314-x (2025).
28. Pettersen, E. F. et al. UCSF Chimera—a visualization system for exploratory research and analysis. *J. Comput. Chem.* **25** (13), 1605–1612. https://doi.org/10.1002/jcc.20084 (2004).
29. Ranković, B. *Lichen secondary metabolites, Bioactive properties and pharmaceutical potential* (Springer, 2019). https://doi.org/10.1007/978-3-030-16814-8
30. Siegel, R. L., Giaquinto, A. N. & Jemal, A. Cancer statistics. *CA Cancer J. Clin.* **74** (1), 12–49. https://doi.org/10.3322/caac.21820 (2024).
31. Solárová, Z. et al. Anticancer potential of lichens' secondary metabolites. *Biomolecules* **10** (1), 87. https://doi.org/10.3390/biom10010087 (2020).
32. Spribille, T., Resl, P., Stanton, D. E. & Tagirdzhanova, G. Evolutionary biology of lichen symbioses. *New. Phytol*. **234** (5), 1566–1582. https://doi.org/10.1111/nph.18048 (2022).
33. Stanojković, T. Investigations of lichen secondary metabolites with potential anticancer activity. In: Lichen secondary metabolites, bioactive properties and pharmaceutical potential, 2rd edn. Springer, Switzerland, 155–174. https://doi.org/10.1007/978-3-030-16814-8_5 (2019).
34. Steinová, J., Škaloud, P., Yahr, R., Bestová, H. & Muggia, L. Reproductive and dispersal strategies shape the diversity of mycobiont-photobiont association in *Cladonia* lichens. *Mol. Phylogenet Evol.* **134**, 226–237. https://doi.org/10.1016/j.ympev.2019.02.014 (2019).
35. Sung, H. et al. Global cancer statistics 2020: GLOBOCAN estimates of incidence and mortality worldwide for 36 cancers in 185 countries. *CA Cancer J. Clin.* **71** (3), 209–249. https://doi.org/10.3322/caac.21660 (2021).
36. Suresh, A. B. & Nadumane, V. K. Identification of Atraric Acid from the Lichen *Ramalina farinacea* and its Anticancer Mechanisms in HepG2, MCF-7, and HeLa Cell Lines in vitro. *Pharmacol. Res. - Nat. Prod.* **10**, 100575. https://doi.org/10.1016/j.prenap.2026.100575 (2026).
37. Tripathi, A. H. et al. K. A review of anti-cancer and related properties of lichen-extracts and metabolites. *Anti-Cancer Agents Med. Chem.* **22** (1), 115–142.

https://doi.org/10.2174/1871520621666210322094647 (2022).

38. Tripp, E. A. & Lendemer, J. C. Twenty-seven modes of reproduction in the obligate lichen symbiosis. *Brittonia* **70**, 1–14. https://doi.org/10.1007/s12228-017-9500-6 (2018).
39. Turanlı, B. Rahim ağzı kanser alt-tiplerine özgü moleküler hedef, biyoişaretçi adaylar ve yeniden konumlandırılan ilaçların belirlenmesi. *Int. J. Adv. Eng. Pure Sci.* **33** (4), 537–548. https://doi.org/10.7240/jeps.869943 (2021).
40. Zhang, Z. et al. Targeting WEE1 kinase for breast cancer therapeutics: an update. *Int. J. Mol. Sci.* **26** (12), 5701. https://doi.org/10.3390/ijms26125701 (2025).

Figures



Figure 1

Morphological and ecological characterization of the study material. A macroscopic photograph representing the vegetative thallus and growth patterns of the *Flavoparmelia caperata* lichen specimen, which was collected from its natural habitat on Fagus orientalis in the Yenice Forests, Karabük, Türkiye.

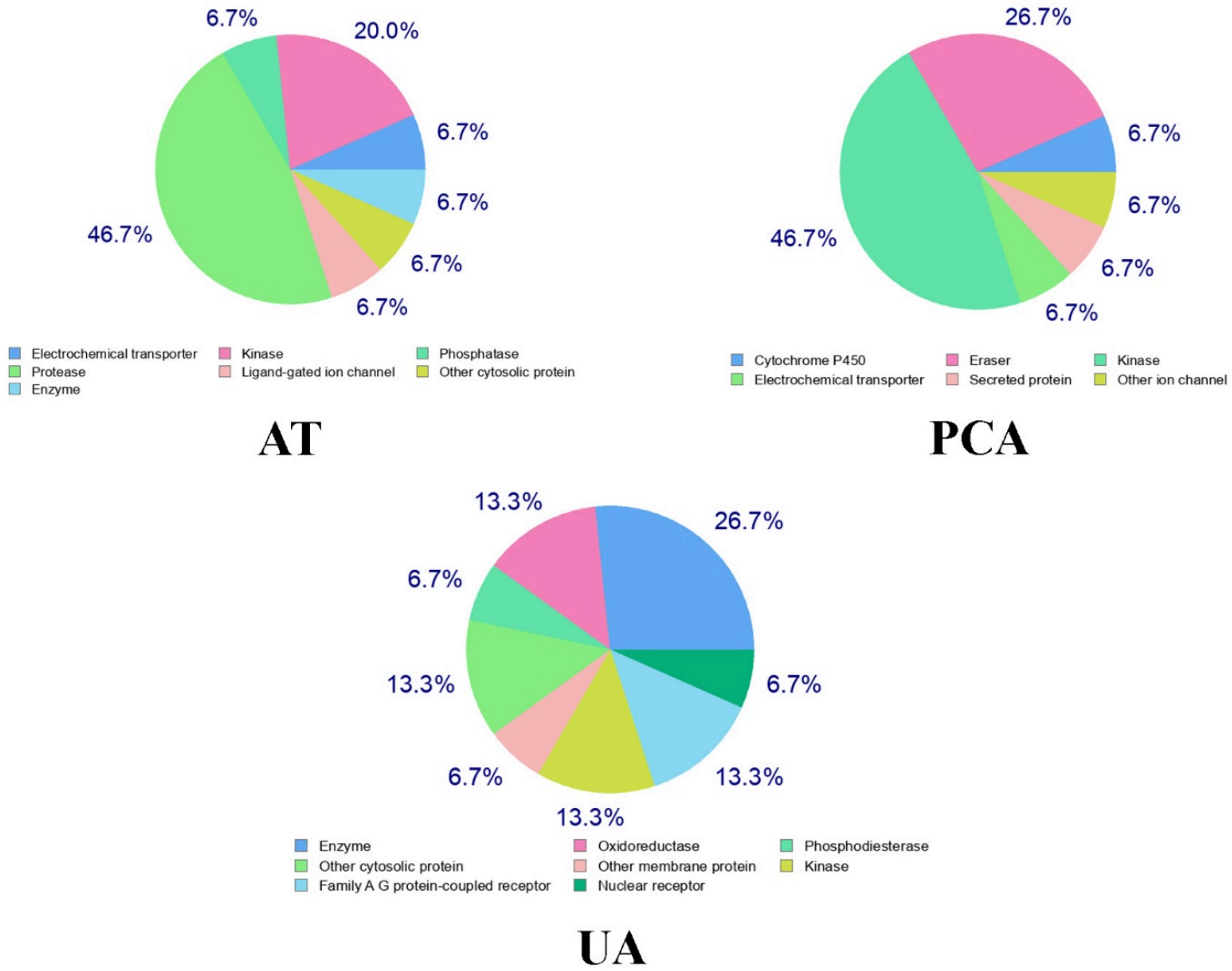


Figure 2

Target prediction analysis for the identified lichen secondary metabolites. Predicted biological target distribution of the studied lichen acids (UA, AT, and PCA) on the basis of SwissTargetPrediction analysis showing the shared affinity for the kinase family.

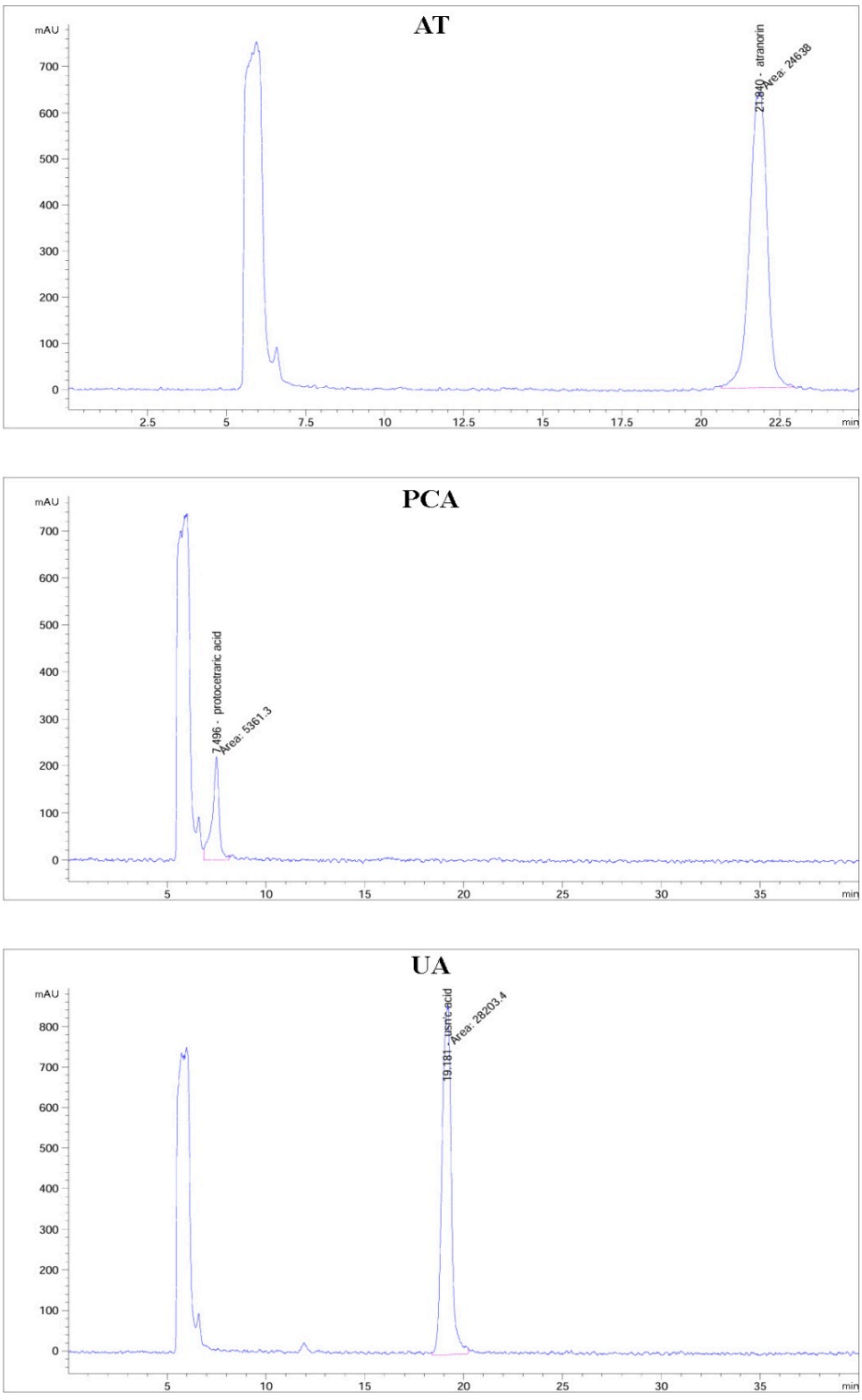


Figure 3

High-performance liquid chromatography (HPLC) chromatogram of the *Flavoparmelia caperata*methanol extract. The figure shows the separation and identification of major lichen acids; peak 1: protocetraric acid (PCA), peak 2: atranorin (AT), and peak 3: usnic acid (UA), recorded at a specific wavelength to confirm the chemical composition.

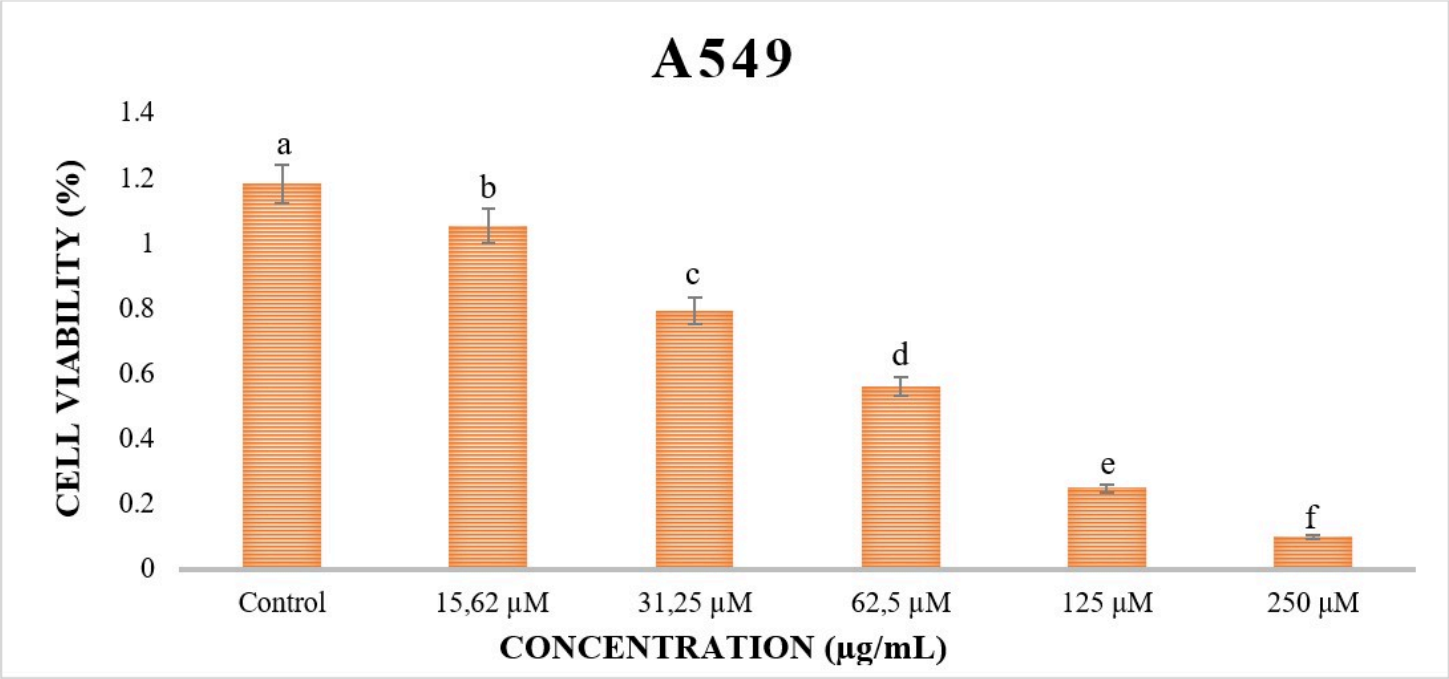


Figure 4

Inhibitory effect of *Flavoparmelia caperata* extract on A549 lung cancer cell viability. A dose–response curve showing the percentage of viable A549 cells following 24-hour treatment with concentrations ranging from 15.62 to 250 µg/mL revealed a significant decrease in survival as the concentration increased.

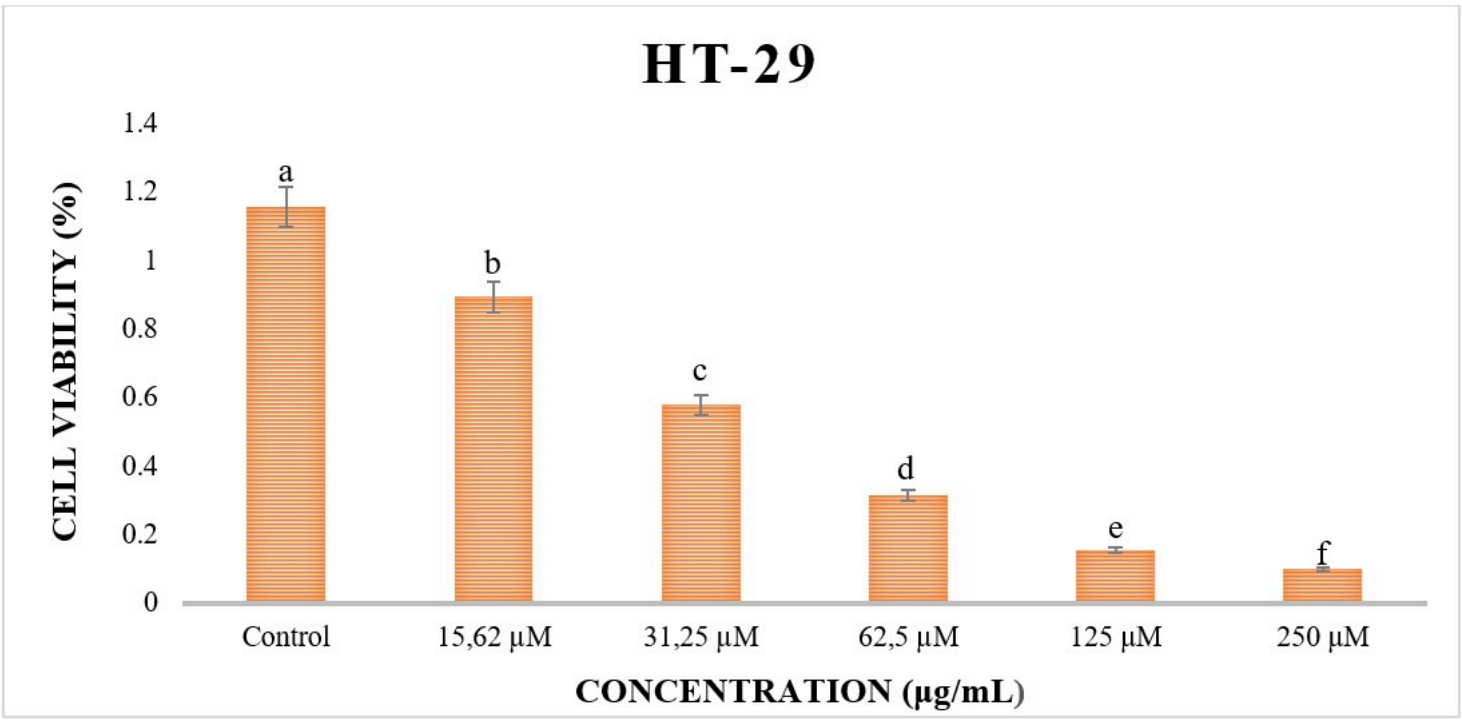


Figure 5

Inhibitory effect of *Flavoparmelia caperata* extract on HT-29 colorectal adenocarcinoma cell viability. A dose–response curve showing the percentage of viable HT-29 cells following 24-hour treatment with concentrations ranging from 15.62 to 250 µg/mL revealed a significant decrease in survival as the concentration increased.

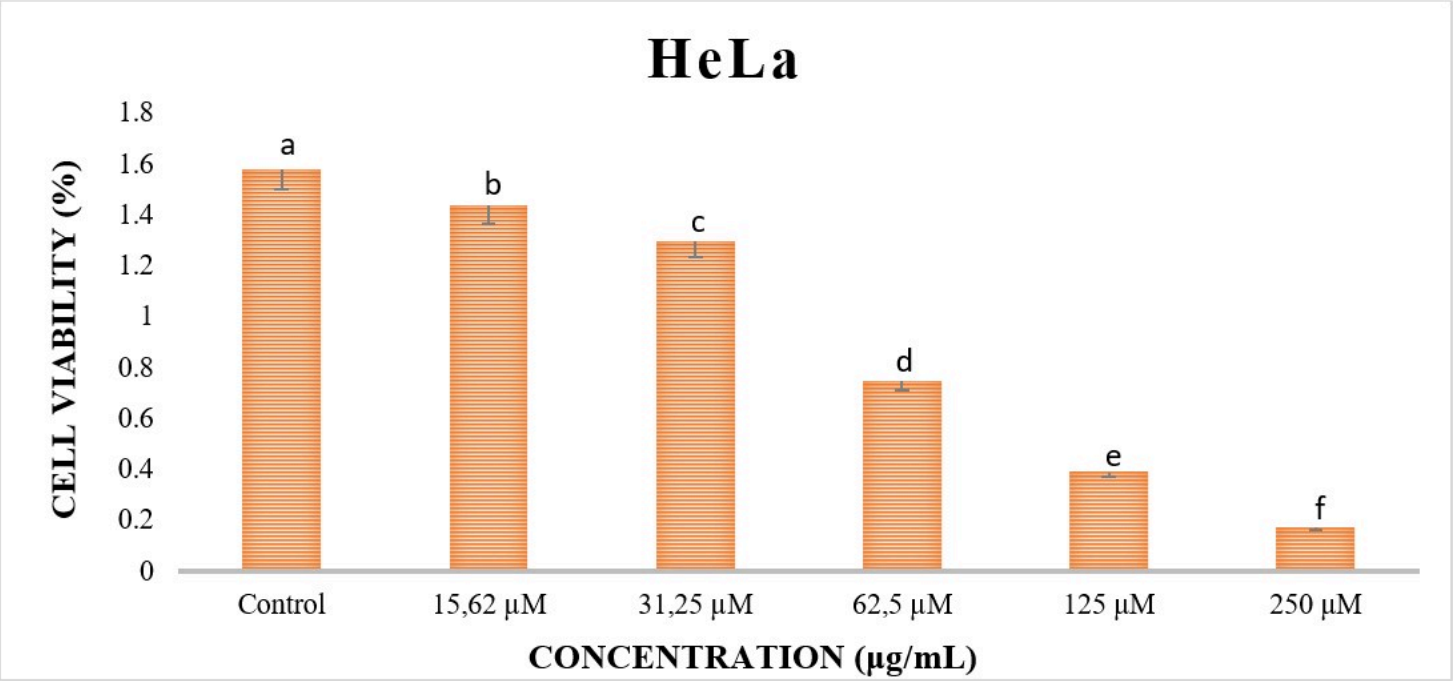


Figure 6

Inhibitory effect of *Flavoparmelia caperata* extract on HeLa cervical cancer cell viability. A dose–response curve displaying the percentage of viable HeLa cells following 24-hour treatment with concentrations ranging from 15.62 to 250 µg/mL revealed a significant decrease in survival as the concentration increased.

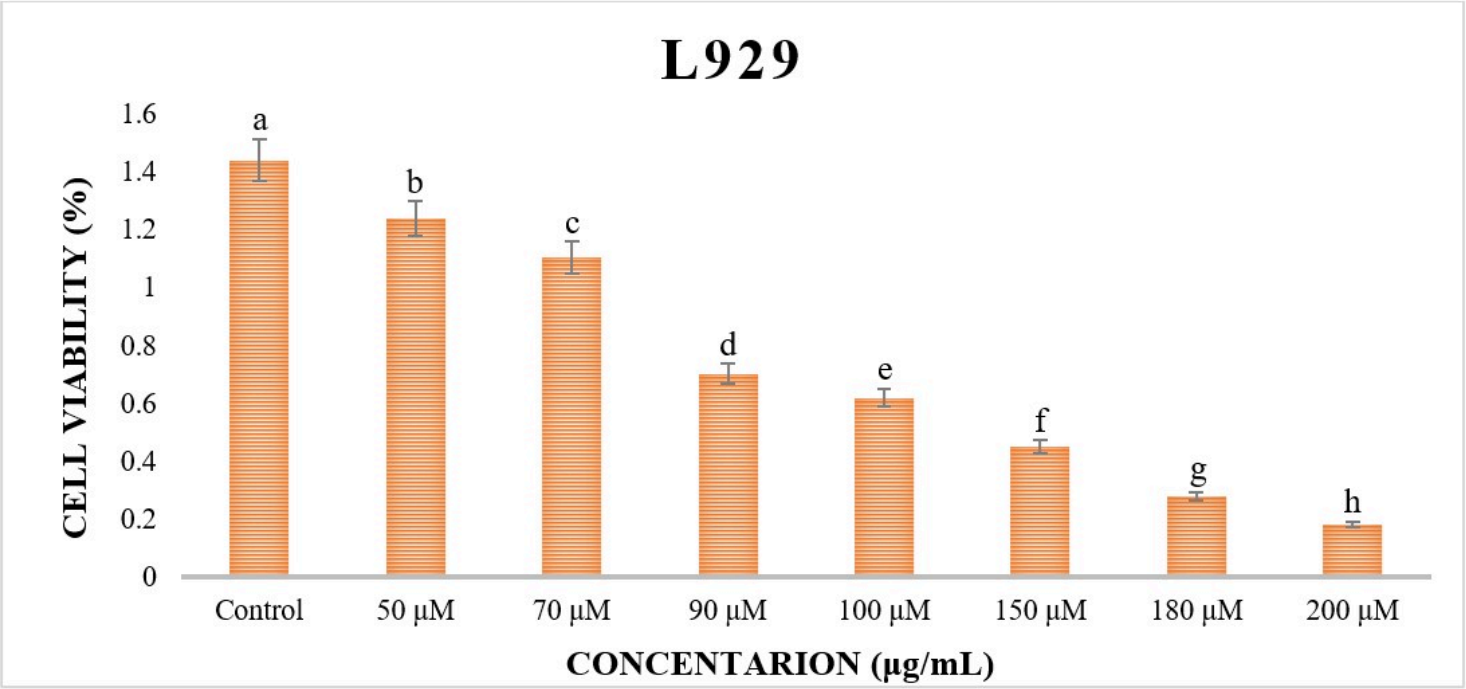


Figure 7

Inhibitory effect of *Flavoparmelia caperata* extract on L929 cell viability. A dose–response curve displaying the percentage of viable L929 cells following 24-hour treatment with concentrations ranging from 50 to 200 µg/mL revealed a significant decrease in survival as the concentration increased.

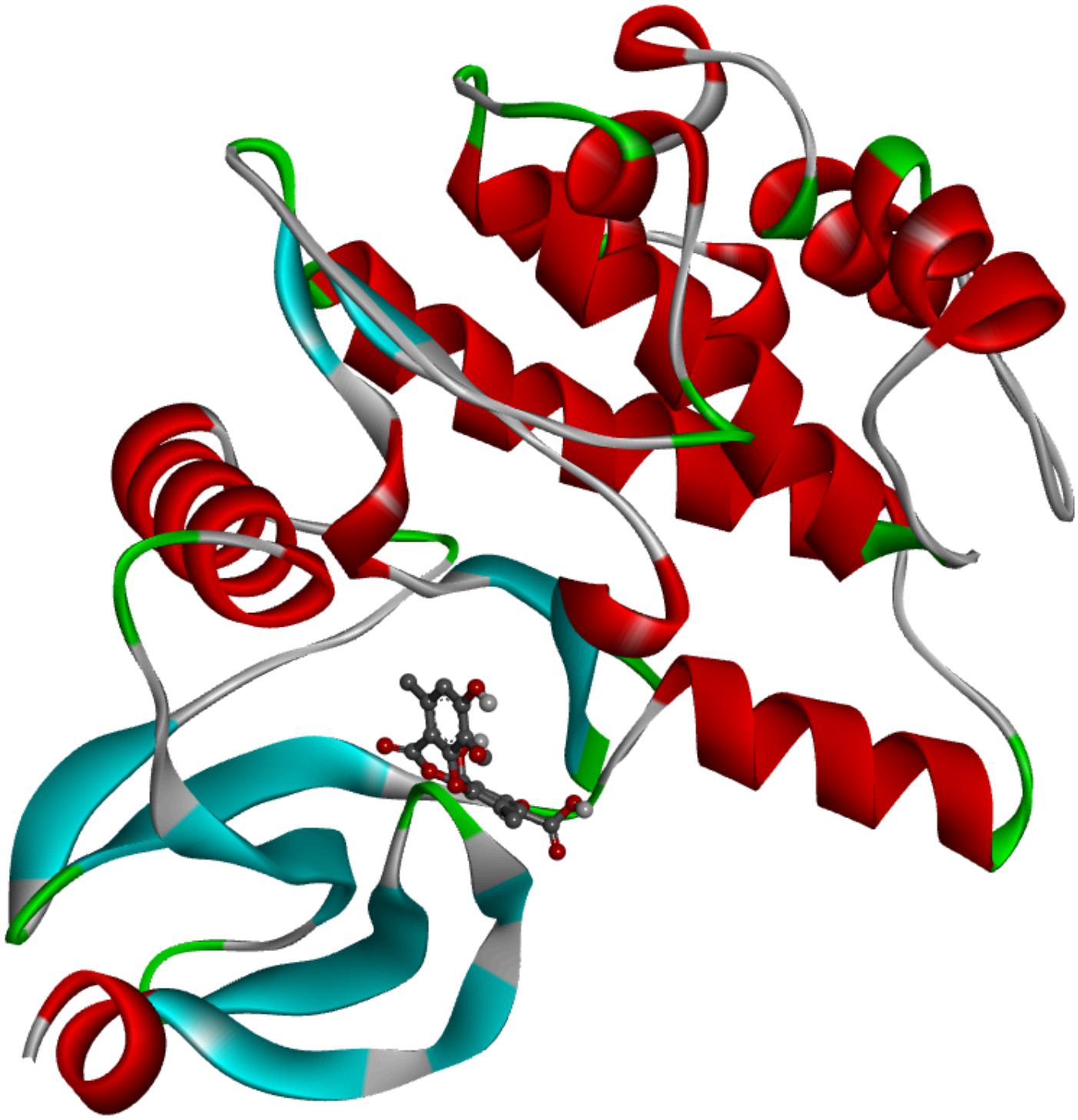


Figure 8

Three-dimensional (3D) molecular docking pose of protocetraric acid within human WEE1 kinase. Visualization of the lowest energy binding conformation of protocetraric acid into the ATP-binding pocket of WEE1 (PDB ID: 8BJU), highlighting its orientation and structural fit.

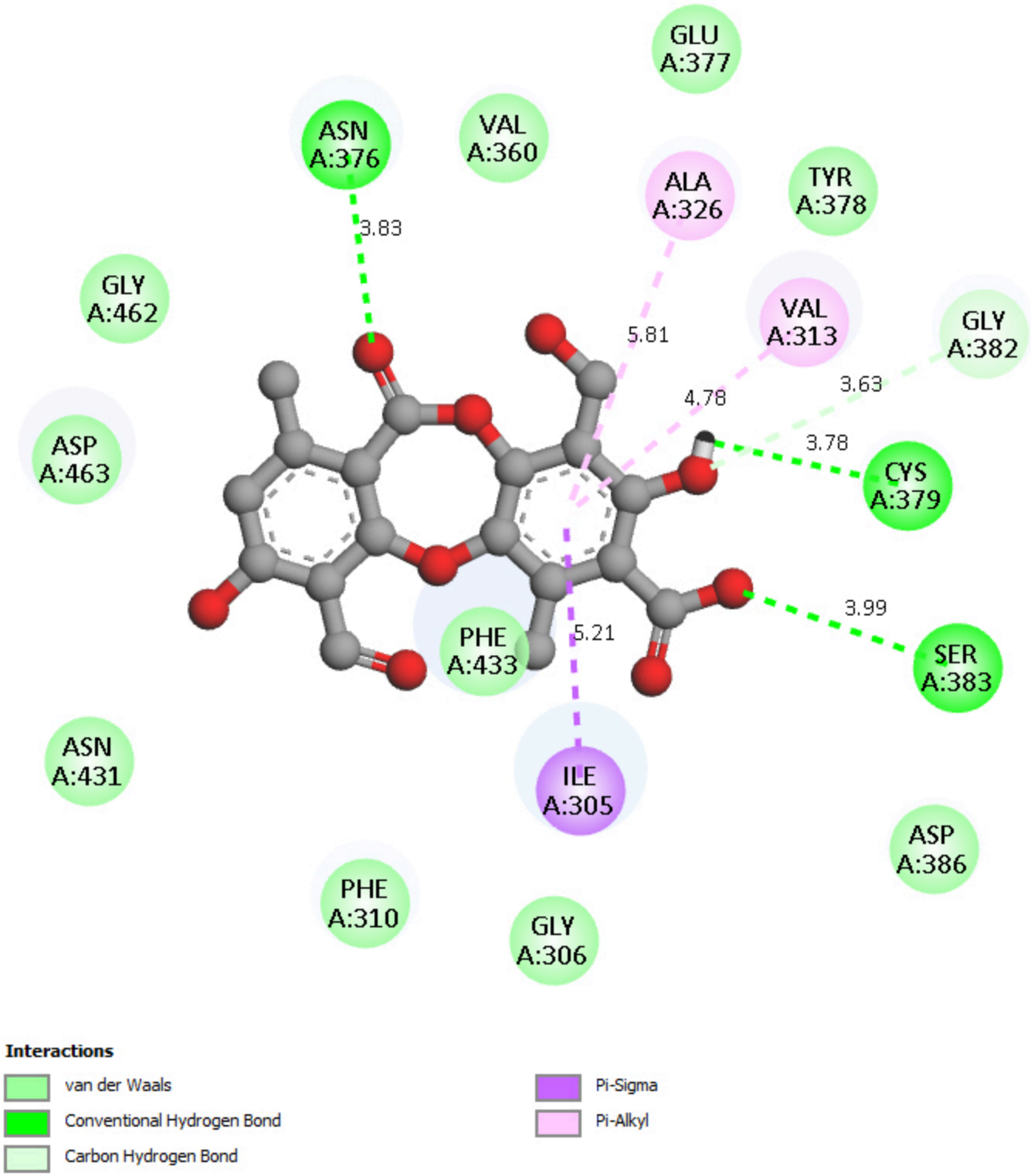


Figure 9

Molecular docking of protocetraric acid with WEE1 kinase (8BJU); 2D interaction diagram. A detailed schematic showing the specific amino acid residues involved in hydrogen bonding, Pi-alkyl interactions, and van der Waals interactions that stabilize the PCA ligand within the catalytic site.

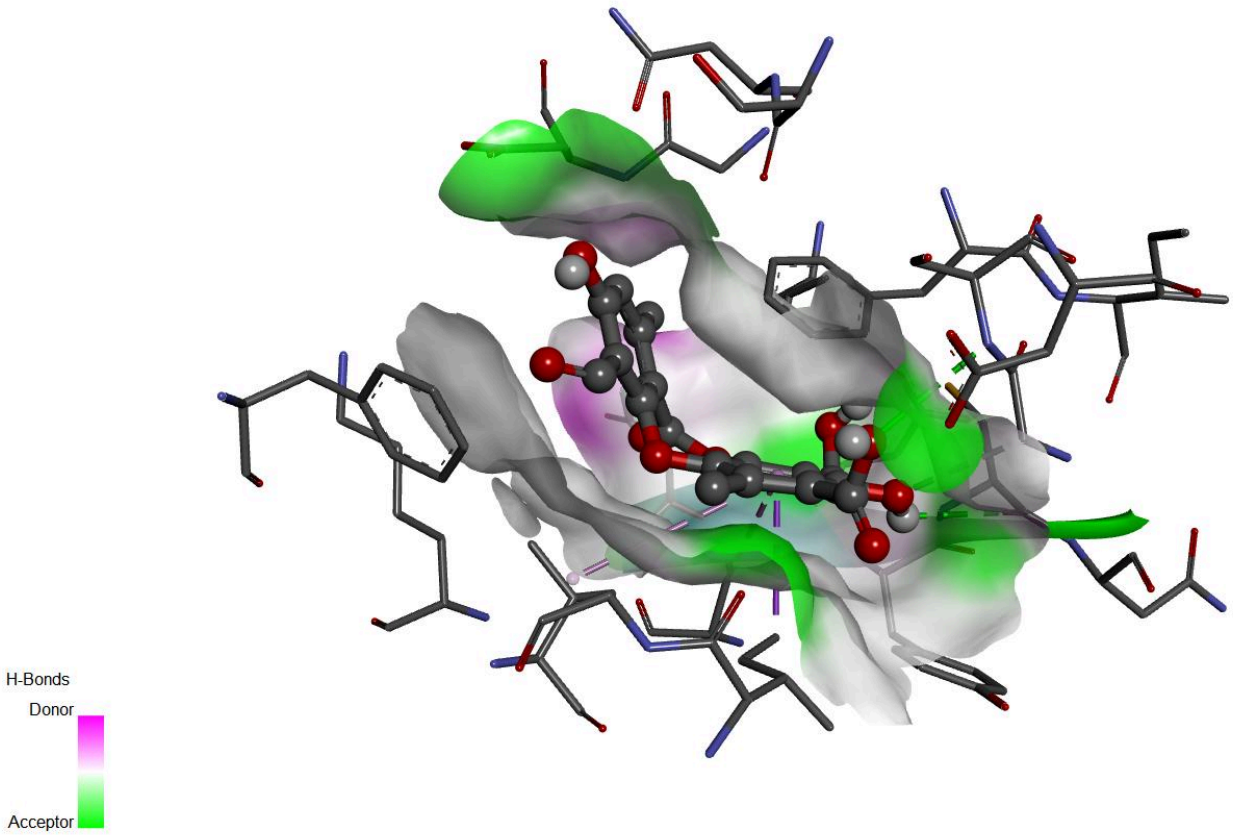


Figure 10

Molecular docking of protocetraric acid with WEE1 kinase (8BJU): Hydrogen bond surface visualization. A molecular surface representation of human WEE1 kinase, which displays the hydrophobicity and hydrogen-bonding acceptor regions occupied by the protocetraric acid molecule.

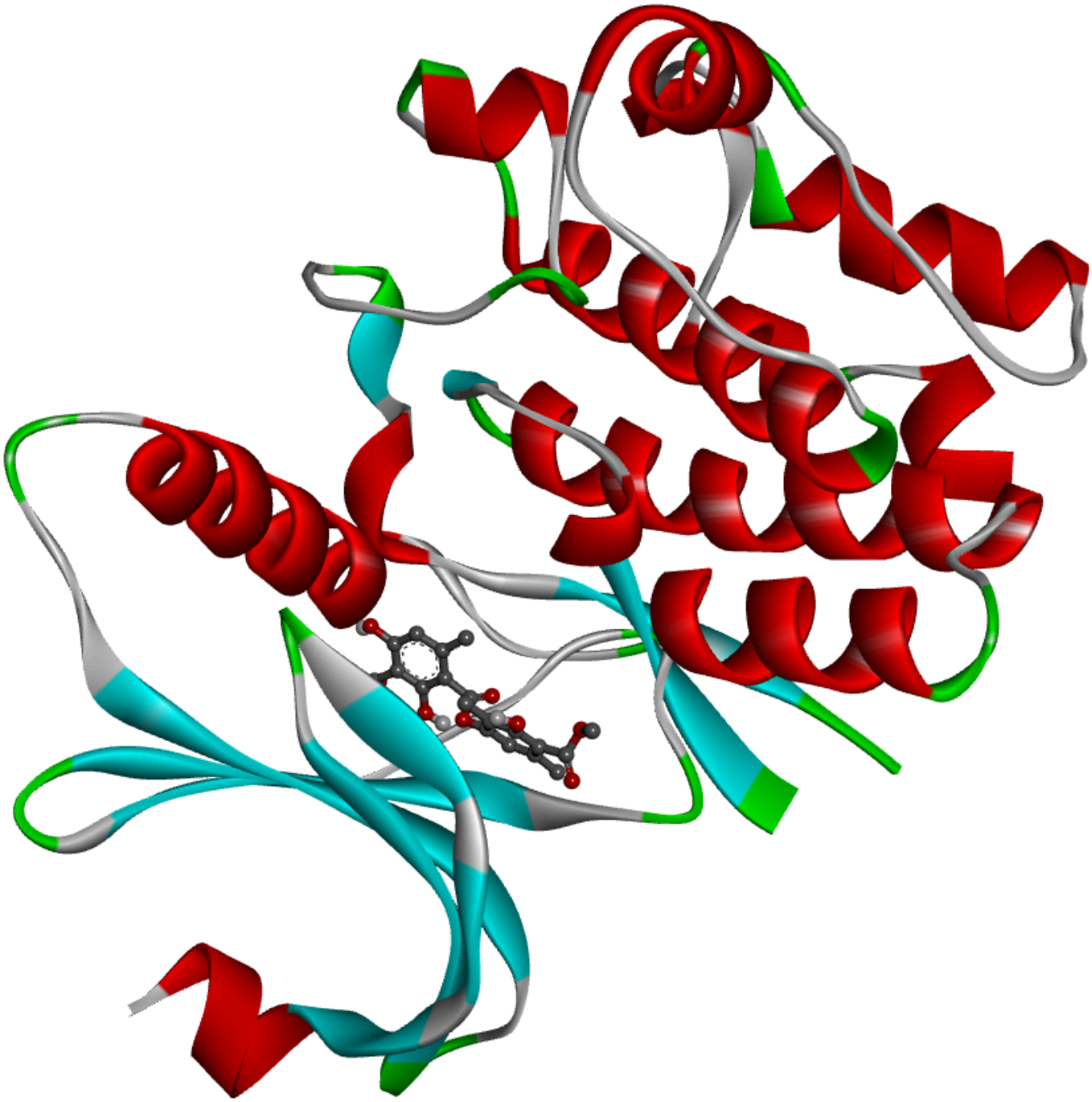


Figure 11

Three-dimensional (3D) molecular docking pose of atranorin within the human WEE1 kinase. Visualization of the lowest energy binding conformation of atranorin in the ATP-binding pocket of WEE1 (PDB ID: 8BJU), highlighting its orientation and structural fit.

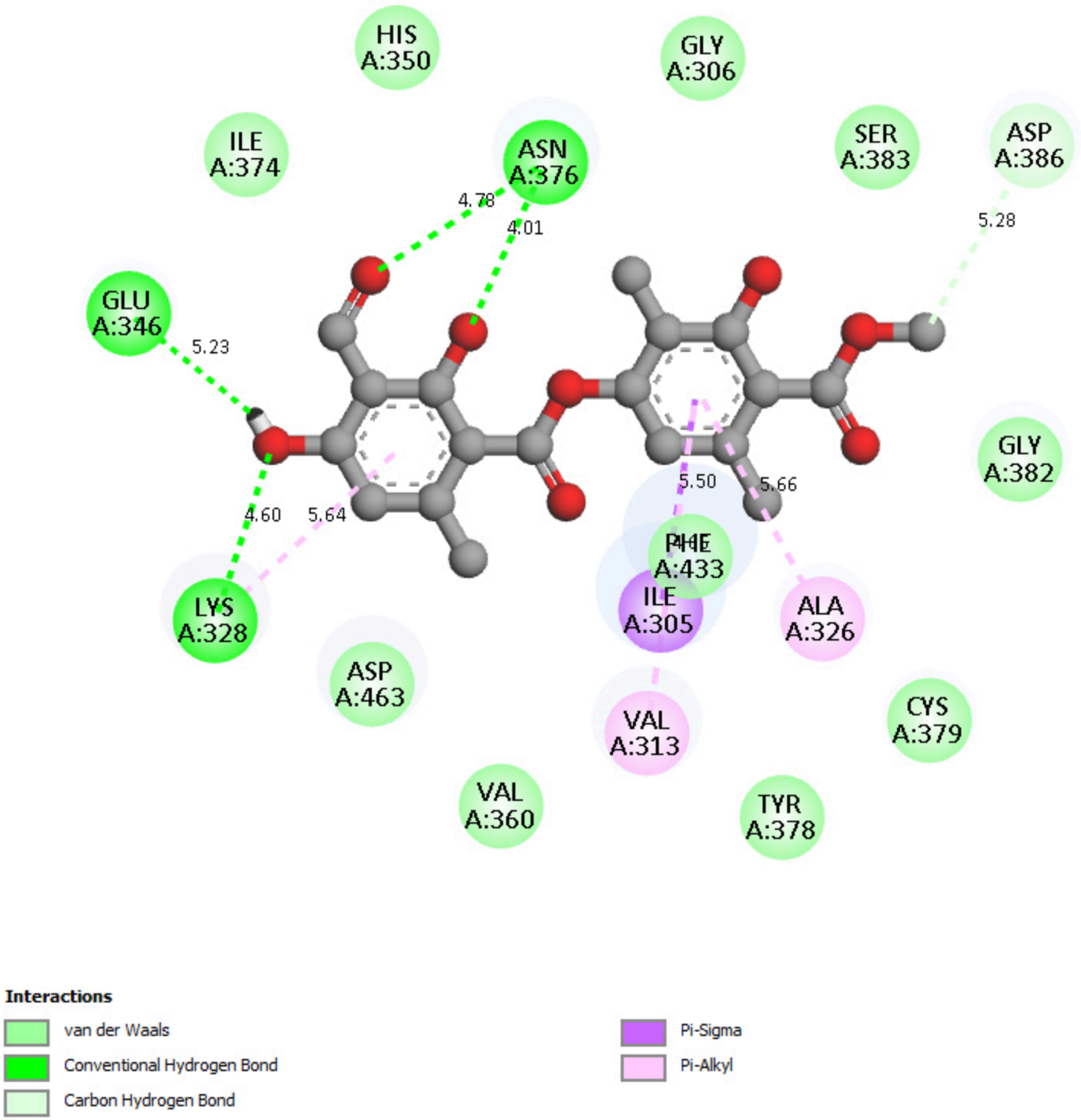


Figure 12

Molecular docking of atranorin with WEE1 kinase (8BJU); 2D interaction diagram. A detailed schematic showing the specific amino acid residues involved in hydrogen bonding; Pi-alkyl, Pi-sigma, and van der Waals interactions; and specific interactions, such as hydrogen bonds with ASN376, GLU346, and LYS328, that stabilize the AT-ligand within the catalytic site.

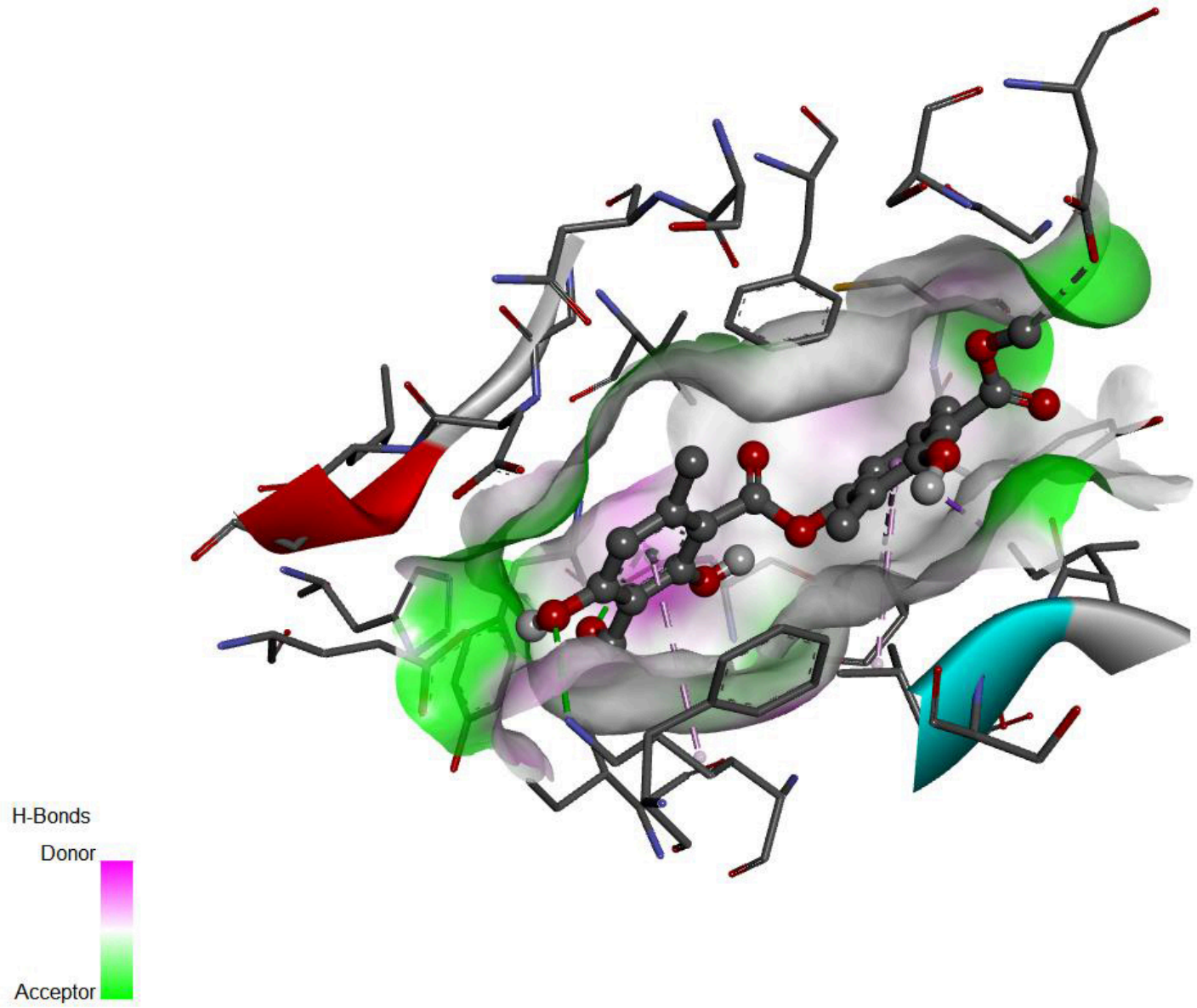


Figure 13

Molecular docking of atranorin with WEE1 kinase (8BJU): Hydrogen bond surface visualization. Molecular surface representation of the human WEE1 kinase, which displays hydrophobicity and hydrogen-bonding acceptor regions occupied by the atranorin molecule.

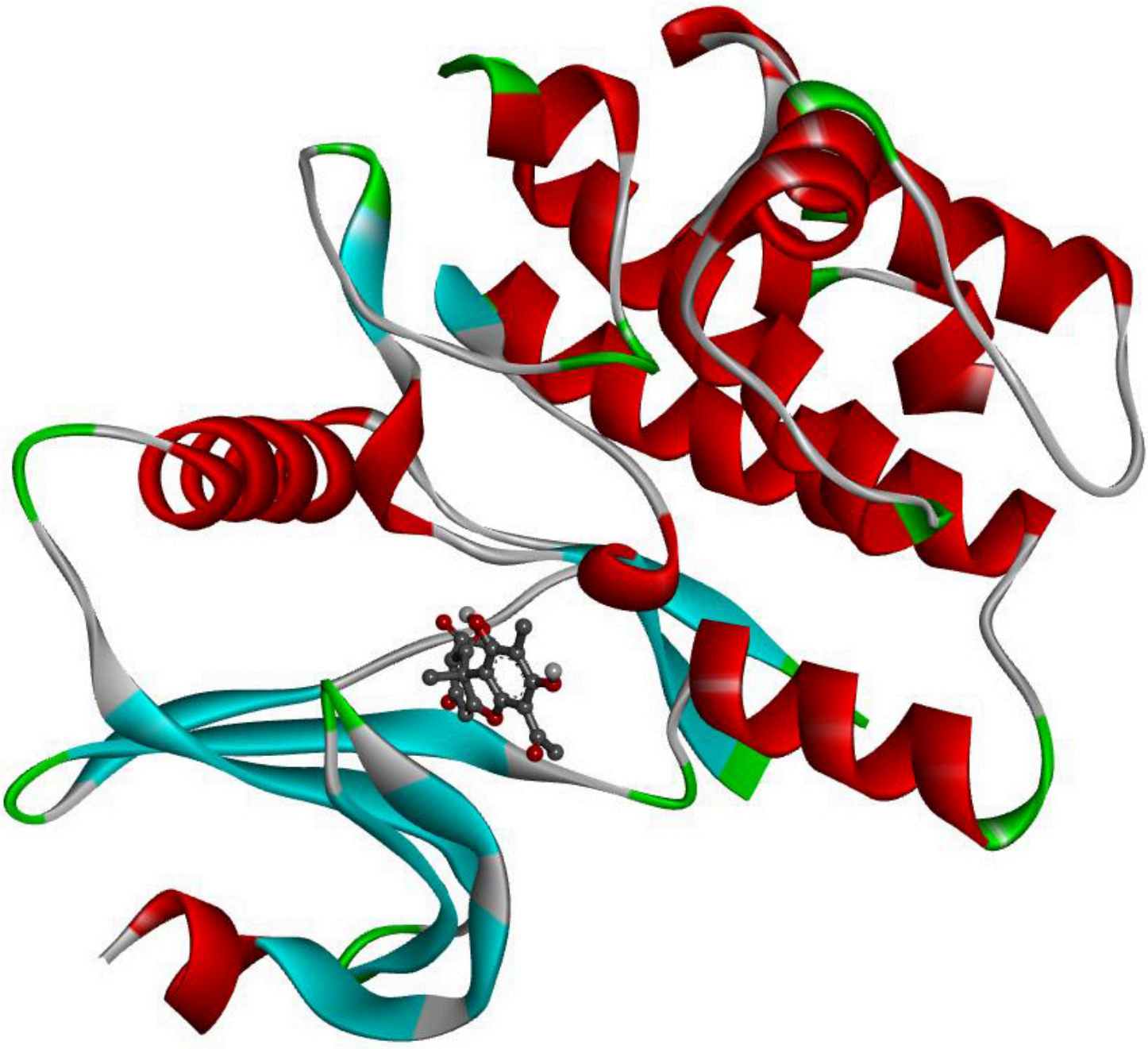


Figure 14

Three-dimensional (3D) molecular docking pose of usnic acid within the human WEE1 kinase. Visualization of the lowest energy binding conformation of usnic acid in the ATP-binding pocket of WEE1 (PDB ID: 8BJU), highlighting its orientation and structural fit.

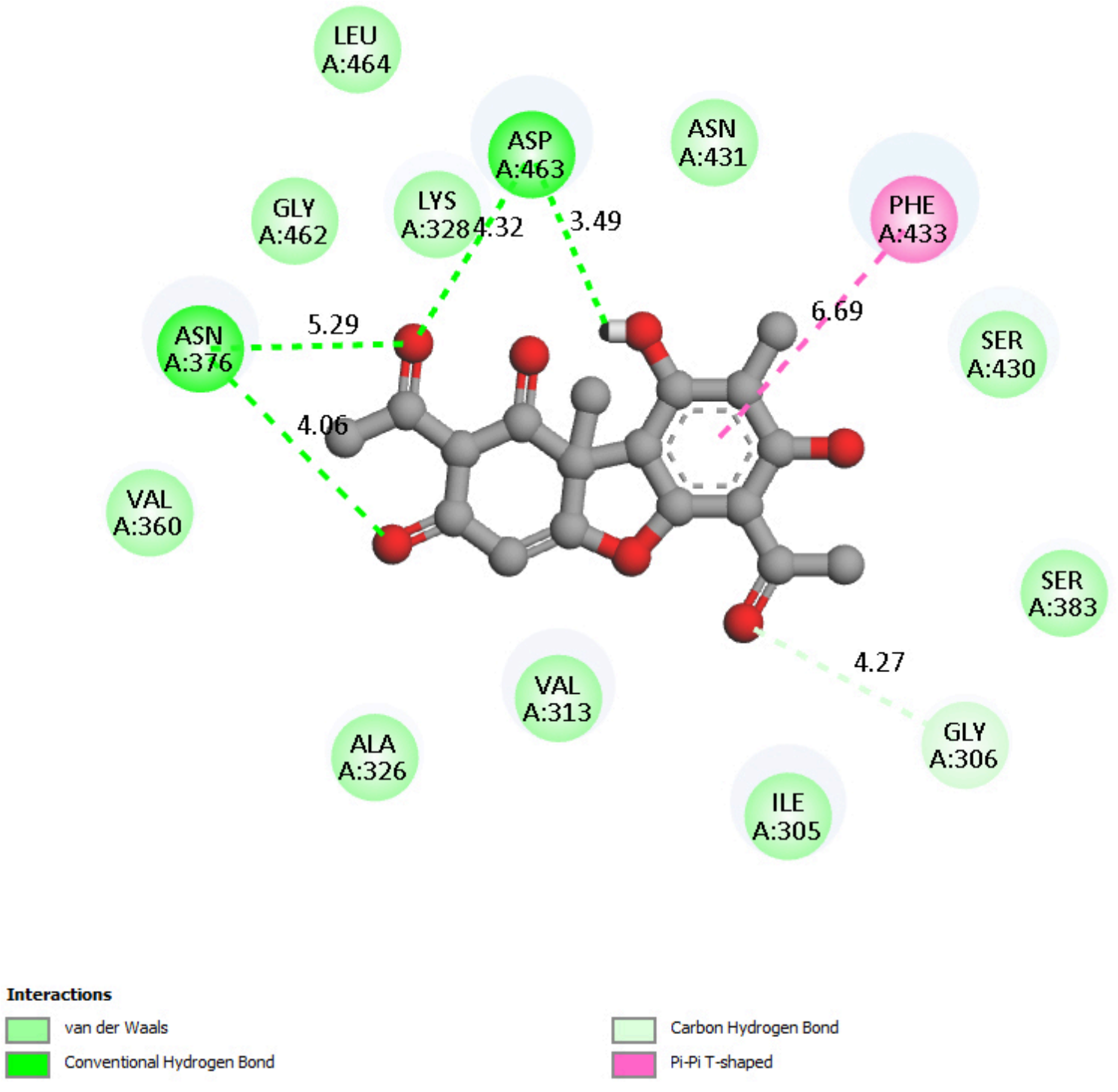


Figure 15

Molecular docking of usnic acid with WEE1 kinase (8BJU); 2D interaction diagram. A detailed schematic showing the specific amino acid residues involved in hydrogen bonding, Pi—Pi T-shaped interactions, and van der Waals interactions and specific interactions, such as hydrogen bonds with ASN376 and ASP3463, that stabilize the UA-ligand within the catalytic site.

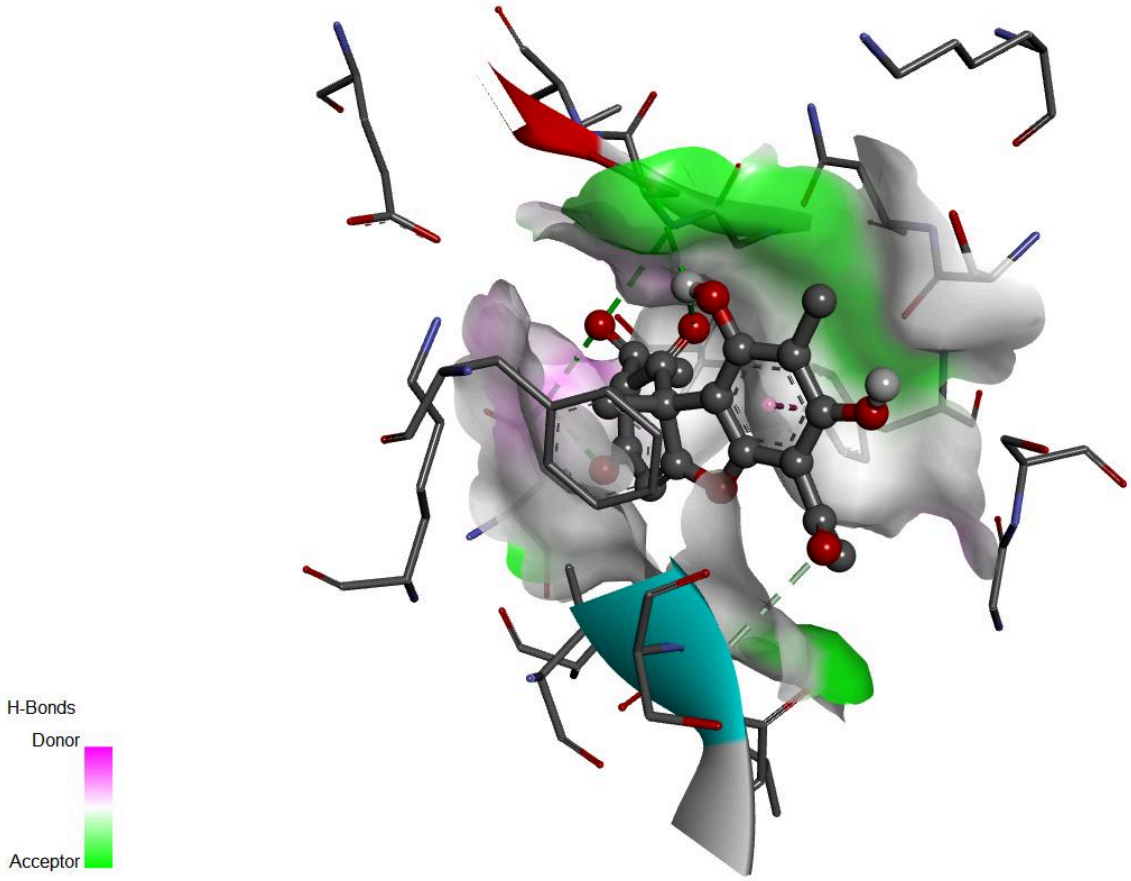


Figure 16

Molecular docking of usnic acid with WEE1 kinase (8BJU): hydrogen bond surface visualization. Molecular surface representation of human WEE1 kinase, which displays the hydrophobicity and hydrogen-bonding acceptor regions occupied by the usnic acid molecule.

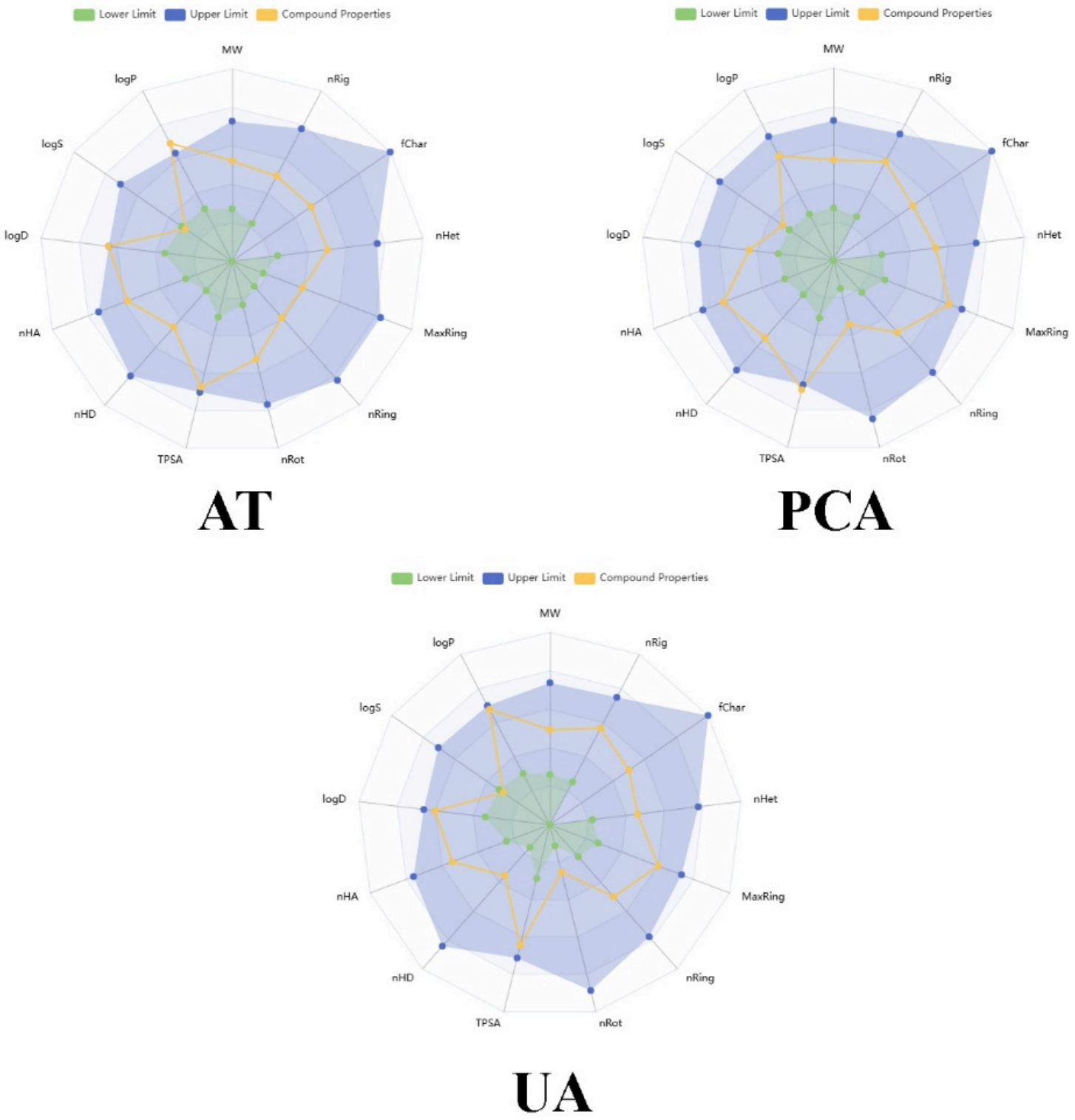


Figure 17

Biosensitivities of the physicochemical properties of atranorin (AT), protocetraric acid (PCA), and usnic acid (UA). Comparative radar charts were used to assess six physicochemical properties, namely, lipophilicity, size, polarity, solubility, flexibility, and saturation, to evaluate the drug likeness of the compounds for oral administration.

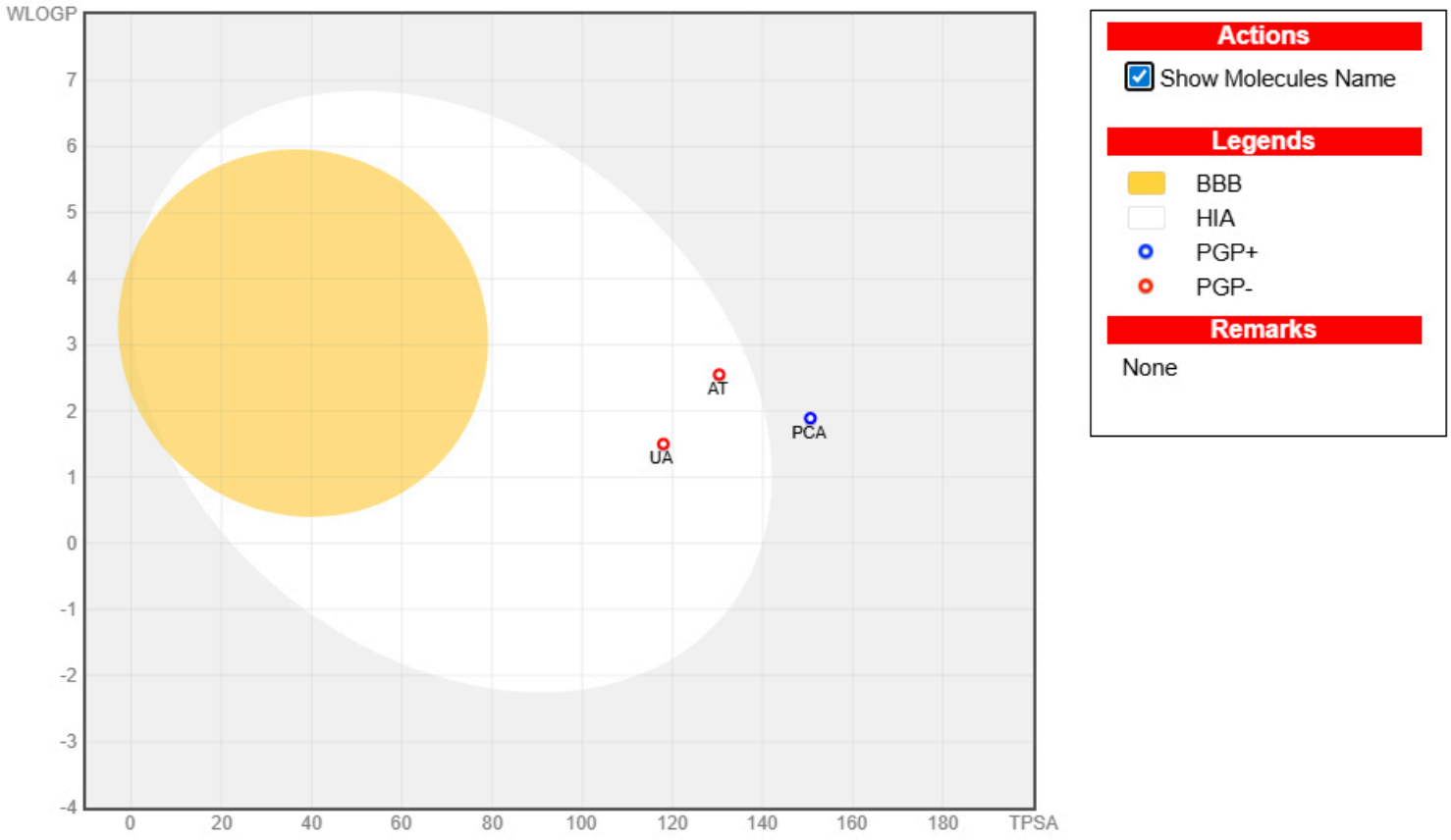


Figure 18

BOILED-Egg model for predicting gastrointestinal absorption and brain penetration. A graphical representation (WLOGP vs. TPSA) estimating the probability of atranorin (AT), protocetraric acid (PCA), and usnic acid (UA) crossing the blood–brain barrier (BBB) and being absorbed in the human digestive system.